Influence of Alkaline Earth Metal Ions on Structures and Luminescent Properties of NamMnUO2(CO3)3 (4-m-2n)- (M = Mg, Ca; m , n = 0–2): Time-Resolved Fluorescence Spectroscopy and Ab Initio Studies

Hanna Oher, Thomas Vercouter, Florent Réal, Chengming Shang, Pascal E Reiller, Valérie Vallet

Influence of alkaline earth metal ions on structures and luminescent properties of $Na_mM_nUO_2(CO_3)_3^{(4-m-2n)-}$ (M = Mg, Ca; m, n = 0-2): time-resolved fluorescence spectroscopy and *ab initio* studies

Hanna Oher[†,‡], Thomas Vercouter[,†], Florent Réal[‡], Chengming Shang[†], Pascal E. Reiller[†], and Valérie Vallet[*,‡]*

† DEN-Service d'Études Analytiques et de Réactivité des Surfaces (SEARS), CEA, Université Paris-Saclay, F-91191 Gif-sur-Yvette, France

‡ Université de Lille, CNRS, UMR 8523 – PhLAM – Physique des Lasers Atomes et Molécules, F-59000 Lille, France

ABSTRACT

The luminescence spectra of triscarbonatouranyl complexes were determined by experimental and theoretical methods. Time-resolved laser-induced fluorescence spectroscopy (TRLFS) was used to monitor spectra of uranyl bicarbonate solutions at 0.1 mol kg_w^{-1} ionic strength and pH ca. 8. The concentrations of Mg^{2+} and Ca^{2+} in the samples were chosen in order to vary the proportions of the alkaline earth ternary uranyl complexes $MgUO_2(CO_3)_3^{2-}$, $CaUO_2(CO_3)_3^{2-}$, and $Ca_2UO_2(CO_3)_3$.

The luminescence spectrum of each complex was determined by decomposition in order to compare with the simulated spectra of model structures $Na_mM_nUO_2(CO_3)_3^{(4-m-2n)-}$ (M = Mg, Ca; m, n = 0-2) obtained by quantum chemical methods. The Density Functional Theory (DFT) and time-dependent (TD)-DFT methods were used with the PBE0 functional to optimize the structures in the ground and excited states, respectively, including relativistic effects at the spin-free level, and water solvent effects using a continuum polarizable conductor model (CPCM). The changes in the structural parameters were quantified with respect to the nature and the amount of alkaline earth counterions to explain the luminescence spectra behavior. The first low-lying excited state was successfully computed, together with the vibrational harmonic frequencies. The DFT calculations confirmed that uranyl luminescence originates from electronic transitions from one of the four non-bonding 5f orbitals of uranium to an orbital that has a uranyl-σ (5f, 6d) character mixed with the 2p atomic orbitals of the carbonate oxygens. Additional single-point calculations using the more accurate TD-DFT/CAM-B3LYP allow to determine the position of the luminescence "hot band" for each structure in the range 467-476 nm, and compared fairly well with experimental reports at around 465 nm. The complete luminescence spectra were built from theoretical results with the corresponding assignment of the electronic transitions and vibronic modes involved, mainly the $U\text{-}O_{ax}$ stretching mode. The resulting calculated spectra showed a very good agreement with experimental band positions and band spacing attributed to $MgUO_2(CO_3)_3^{2-}$, $CaUO_2(CO_3)_3^{2-}$, and $Ca_2UO_2(CO_3)_3$. The evolution of luminescence intensities with the number of alkaline earth metal ions in the structure was also correctly reproduced.

INTRODUCTION

After light excitation in the UV or visible range, most uranium(VI) compounds produce luminescence in the energy range 15 000 – 22 000 cm^{-1} (650-450 nm), which has been extensively

studied since the spectra are fingerprints of the coordination of the uranyl ion UO_2^{2+}. The positions of the luminescence bands, band spacings, bandwidths, and intensities are features that can be interpreted to determine the nature and number of ligands in the first coordination layer of UO_2^{2+}, and the local symmetry of the complex. This information is looked for by chemists in order to give the best description of uranium speciation both in solutions and in solids. Time-resolved laser-induced fluorescence spectroscopy (TRLFS) has been widely used for the identification and characterization of U(VI) compounds since it is a non-intrusive, sensitive, and selective technique to detect the luminescence of U(VI) species, even with traces of uranium.[1,2] The main spectroscopic features are usually reported in the literature and spectral attributions have been proposed for many aqueous inorganic complexes[3–9] and minerals.[10–18]

The case of the carbonate species is particularly interesting.[8,13,15,19–21] Both anionic complexes $UO_2(CO_3)_2^{2-}$ and $UO_2(CO_3)_3^{4-}$ are characterized by an absorption spectrum shifted to longer wavelengths as compared with UO_2^{2+} aqua ion and its hydrolyzed species.[22,23] Meinrath et al. reported 20 years ago that the luminescence of $UO_2(CO_3)_2^{2-}$ seemed to be too weak to be easily observed.[4] Conversely, recent works have shown that the use of modern TRLFS set-up allows measuring $UO_2(CO_3)_3^{4-}$ at ambient temperature.[21,24] It has been shown that the U(VI) luminescence is increasing when alkaline earth metal ions are added into a solution that contains $UO_2(CO_3)_3^{4-}$, *i.e.,* in the presence of dissolved bicarbonate. The repartition of these species (and solids) can be described in e.g. a $\log_{10}(a(HCO_3^-)/a(H^+))$ vs. $\log_{10}(a(Ca^{2+})/a(H^+)^2)$ plan for Ca. There was a direct evidence of the formation of ternary complexes $CaUO_2(CO_3)_3^{2-}$ and $Ca_2UO_2(CO_3)_3$ where the calcium ions enter the second coordination layer of the uranyl and interact with the carbonate ligands, as first reported by Bernhard et al.,[25] and investigated later on by several groups.[8,19,21,26–31]

The luminescence of such complexes exhibits a hypsochromic shift of the whole spectrum by about 300 cm^{-1} compared with the free ion, when most other U(VI) compounds, like phosphates, silicates, hydroxides, or organic complexes, are showing a bathochromic shift. The blue-shifted luminescence of the triscarbonatouranyl(VI) entities results from the strong interaction of UO_2^{2+} with the carbonate ligands that bind the uranium atom with two out of their three oxygens in the equatorial plane of the uranyl ion, leading to a six-fold-coordinated uranyl structure. Thanks to this unusual feature, TRLFS has enabled the direct identification of alkaline earth triscarbonatouranyl carbonate complexes in many different types of waters like e.g., seepage water of mine tailing pile,[25] granitic groundwater,[32] seawater,[33] natural drinking water from wells,[19] and in sediment pore waters of the Hanford contaminated sites.[34]

The reason of the increase of the triscarbonatouranyl species luminescence intensity in presence of calcium is still unclear and may originate from either favorable vibronic coupling or diminution of quenching effects from the carbonate ion. Similar observations have been made with the less stable ternary $MgUO_2(CO_3)_3^{2-}$ and $SrUO_2(CO_3)_3^{2-}$ complexes,[35,36] while the confirmation of the existence of the ternary $Mg_2UO_2(CO_3)_3$ complex is still discussed.[26,31,35]

Quantum chemical modeling is an appropriate theoretical support for a better understanding of the luminescence of these ternary triscarbonatouranyl complexes with alkaline earth metal cations. The luminescence of solid uranyl carbonates has been successfully described and analyzed using periodic density functional theory (DFT), particularly in the case of liebigite $Ca_2UO_2(CO_3)_3 \cdot 11H_2O$ and the dehydrated $Ca_2UO_2(CO_3)_3$ crystal.[37] While it is established that the luminescence of uranyl compounds is related to transitions from $5f_\delta$ and $5f_\phi$ excited levels, the nature of the ground state orbitals still needs to be more precisely defined for the aqueous uranyl carbonate complexes. This constitutes a first objective of the present work with the support of

quantum chemistry modeling. For this aim, triscarbonatouranyl model structures were built with calcium, magnesium and sodium counterions (from 1 to 3 Na^+ depending on the amount of alkaline earth metal present) to maintain the highest symmetry and reduce the total molecular charge.

Investigating luminescence properties from a uranyl complex requires a step-by-step methodology. The geometry of the complexes first needs to be correctly built both in the ground and excited states, which can be checked by comparison with structural studies on triscarbonatouranyl complexes, with and without calcium. On the one hand, structures and atomic distances were determined by X-Ray Diffraction (XRD),[38] and Extended X-ray Absorption Fine Structure (EXAFS)[15,20,35,39,40] both in crystal form and in solution, respectively. Vibration frequencies are also available from measurements by Raman and Infrared spectroscopy.[41–44] On the other hand, theoretical methods were applied to triscarbonatouranyl complex by DFT[45] or hybrid DFT,[46] Quantum Mechanical Charge Field Molecular Dynamics (QMCF-MD),[47] or classical molecular dynamics (MD) simulations.[45,48] Then one needs to calculate and identify the excited states that may be involved in the electronic transitions. TD-DFT has demonstrated its ability to reproduce electronic transitions in uranyl compounds from low-lying excited states, including relativistic effects, electron correlation, and spin-orbit coupling.[49,50] The calculation of the coupling factors between the different vibrational states of the ground and excited states can be achieved using the Franck-Condon approach for dipole-allowed transitions, to finally describe luminescence spectra.

Quantum chemical methods have already been applied to simulate the luminescence properties of uranyl chloride crystals[51] and complexes,[52,53] uranyl fluoride,[54] and uranyl glycine complex.[55] We recently applied a methodology developed by Tecmer et al.,[49] and tested on tetra-halogen compounds $UO_2Cl_4^{2-}$ that resulted in simulated luminescence spectra in good accordance with

experimental data.[50] Our approach based on DFT and time-dependent DFT, offers a good compromise between the accuracy of the calculations and a rather low computational cost, which enables the application of the method to larger molecular assemblies, especially with actinides.

In the present work, we optimized the geometries of the $Na_mM_nUO_2(CO_3)_3^{(m+2n-4)}$ (M=Mg, Ca; m,n = 0-2) complexes by DFT, and compared with literature data to evaluate the reliability of the uranyl distances and harmonic frequencies and their change between the ground and luminescent states to capture the evolution of intensities. The luminescence properties calculated by TD-DFT methods were compared to experimental data acquired with our TRLFS set-up, and from the literature. Finally, the present results from quantum chemical modeling are discussed and provide a better understanding of the luminescence bands and intensities of the ternary alkaline earth metal triscarbonatouranyl complexes.

EXPERIMENTAL DETAILS

Reagents and solution. Five samples of varying [Mg]/([Ca] + [Mg]) ratios from 100% to about 50% were prepared for further acquisition of resulting luminescence signals of $Me_nUO_2(CO_3)_3^{(4-2n)-}$ (Me = Mg^{2+}, Ca^{2+}; n = {1,2}). The ionic strength was fixed at 0.1 mol kg_w^{-1} by dissolving appropriate quantity of anhydrous NaCl (Sigma-Aldrich, ACS reagent, ≥ 99%) in Millipore deionized water (Alpha-Q, 18.2 MΩ · cm). The uranium concentration was of 50 µmol kg_w^{-1} after successive dilutions of concentrated stock solution of natural U(VI) prepared with U_3O_8 solid and 37% hydrochloric acid (Sigma-Aldrich, ACS reagent). Using a hydrogen ion-sensitive glass electrode (Mettler Toledo, USA), the aqueous pH value was maintained ca. 8 for all the sample solutions. In order to maintain the performance accuracy, the four-point calibration with commercial solutions of fixed pH at 1.68, 4.01, 6.87, and 10.01 was daily required. The adjustment of pH 8 was done through the addition of freshly prepared NaOH (Analytical Grade, Fisher) and

diluted HCl solutions. The sodium bicarbonate solution (Analytical Grade, Fisher) was freshly prepared, the introduced quantity of which was calculated based on the chemical equilibrium between the aqueous solution in the absence of alkaline earth metal ions and atmospheric $CO_2(g)$. Calcium chloride (Sigma-Aldrich, ACS reagent, ≥ 99%) and magnesium chloride (Sigma-Aldrich, ACS reagent, ≥ 99%) solutions of various concentrations were used to control the concentration of Ca^{2+} and Mg^{2+}. Reagent preparations in experiments were performed by weighing and measurements of pH values were done in triplicate at 22°C. The aqueous pH values were regularly checked during the preparation and the last check was conducted just before the luminescence measurement.

Luminescence measurements. A 2 mL U(VI) solution aliquot was taken from the prepared test sample and placed in a 1 cm quartz fluorescence cuvette (QS101, Suprasil, Hella Analytics). A preliminary equilibration, period of 10 min at 22°C for the used cuvette has been reached prior to data acquisition using a thermostated sample holder connected to a thermostat with circulating water (Peter Huber Kältemaschinenbau AG, Germany). As described fully elsewhere,[21] the excitation laser beam was generated by a 355 nm tripled Nd:YAG laser (Surelite, Continuum, USA) coupled to an optical parametric oscillator system (Horizon, Continuum, USA), delivering 5 ns pulses at 10 Hz. The excitation wavelength was set at 450 nm, allowing an optimal luminescence signal – proper balance between quantum yield of U(VI) species and laser energy – after a preliminary test. The excitation energy at 450 nm was monitored using a RJP-734 Joule-meter (Laser Probe, Inc, and was about 23 mJ.

A spectrometer (Acton SP-2358i, Roper Scientific) equipped with an intensified CCD camera (iStar DH734-25F-03, Andor Technology) was used to collect the luminescence signal with either a 300 or a 1800 lines mm^{-1} grating . The 300 lines mm^{-1} grating capable of recording the

convolution of various fluorescing components was first selected to measure the full uranyl emission spectra covering the wavelength range of 425 nm to 615 nm with a resolution estimated at 0.2 nm for each sample solution. The 1800 lines mm^{-1} grating providing a resolution estimated at 0.025 nm was then used to focus on specific characteristic peaks with the aim of detecting their possible modifications as a function of Mg/(Ca + Mg) ratios, as well as aqueous compositions in terms of $M_nUO_2(CO_3)_3^{(4-2n)-4}$ species. The time-resolved measurements were carried out at a delay time of D = 25 ns after the laser pulse and during a measurement gate width of W = 1 μs. Each spectrum was the result of signal accumulated over more than 4000 laser shots depending on the grating used.

COMPUTATIONAL DETAILS

The simulation of the luminescence spectra of uranyl complexes were done using the ezSpectrum 3.0[56] program to compute the Franck-Condon factors, corresponding to the overlaps between the luminescent and the ground vibrational wavefunctions. As in our previous work, Duschinksy rotations of the normal modes were included.[50] The numbers of vibrational quanta in excited and ground state were selected to be one and five, respectively to match the number of transitions on experimental spectra. All the stick spectra were computed at 300 K. In order to be able to make a comparison of theoretical results with experimental curves, the calculated peaks were broadened homogeneously using Lorentzian functions with a width corresponding to the experimental values of the full width at half-maximum. For the spectra simulations all data were generated by the *ab initio* packages as described below.

The interactions between uranyl and its first and second coordination spheres might affect the electronic structure of the uranyl unit. In order to keep reasonable computational costs, the *ab initio* calculations were performed on model molecular systems built to represent the triscarbonatouranyl

negatively charged complex charge-compensated by counter cations in its close environment (Fig. 1). In the present study, the triscarbonatouranyl complex was built with three bidentate carbonate ligands in the equatorial plane of the uranyl ion, matching a D_{3h} symmetry (Fig. 1a), as evidenced by EXAFS solution data.[40,57] Then Na^+ counter ions were positioned in between the carbonate ligands. The $Na_3UO_2(CO_3)_3^-$ model complex was first created to reduce the complex total charge to minus one while keeping the D_{3h} symmetry, and taken as a reference structure (Fig. 1b), instead of the bare $UO_2(CO_3)_3^{4-}$ complex, as such a highly charged anion is necessarily stabilized in solution with charge-balancing cations. Then structures in which one or two Na^+ cations are substituted by Ca^{2+} or Mg^{2+} were investigated (Fig. 1c and d, respectively), leading to neutral and mono-charged cationic complex, respectively. The geometries of these model systems were computed with inclusion of solvent effect to imitate experimental conditions.

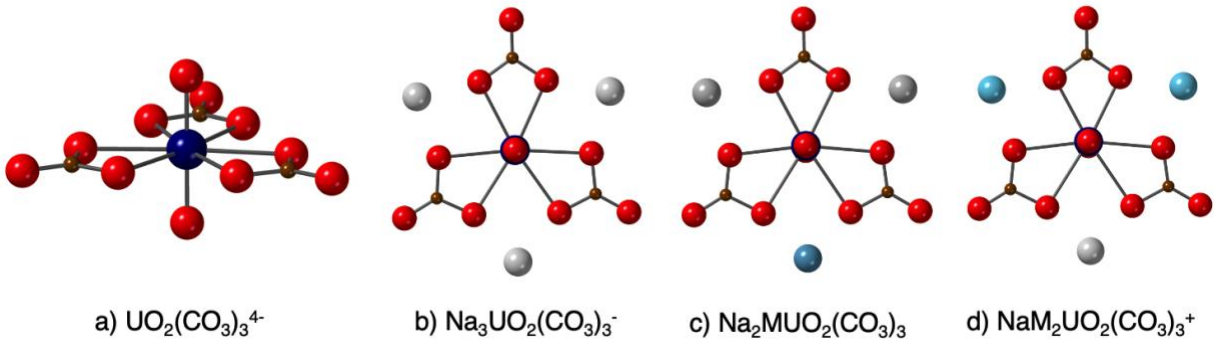

Figure 1. The structures of uranyl bidentate tri-carbonate complexes $Na_mM_nUO_2(CO_3)_3^{(4-m-2n)-}$ (M=Mg, Ca; m,n = 0-2) in water with different composition of the second coordination sphere optimized at the DFT/PBE0 level of theory. In red - O, brown - C, dark blue - U, gray - Na, light blue - Ca, Mg.

The QM methods were used as described and justified in our previous study.[50] All the ground-state and excited-state molecular geometries were optimized including the relativistic effects at the

spin-free level using the PBE0 functional of the density,[58] and accounting for water solvent effects via the CPCM[59] (the permittivity of water $\varepsilon_r = 78.35$). Note that spin-orbit coupling effects (SOC) are not expected to affect uranyl ground and excited state geometries as discussed by Pierloot et al.[60] The structure of the first low-lying excited state was optimized using the time-dependent (TD)-DFT/PBE0 method as implemented in Gaussian 16 code,[59] with equilibrium CPCM solvation. The vibrational harmonic frequencies were computed using an analytic Hessian matrix, and all relaxed geometries considered for the vibronic spectra calculations represent real minima as they have no imaginary frequencies. All optimized structures are available in electronic supplementary information (ESI). In these calculations, the def2-TZVP (second generation of triple-zeta polarization quality) basis sets[61,62] have been used for all light elements i.e., C, O, Na, Mg, and Ca. The uranium atom is described by a small-core Relativistic Effective Core Pseudopotentials (RECP), which accounts for scalar relativistic of the uranium 60 core-electrons,[63,64] and the valence electrons are described by the def-TZVP (first generation of triple-zeta polarization quality) basis set.[65] In the TD-DFT calculations, the Gaussian program defaults for frozen core orbitals were overridden to freeze the U (5s, 5p, 5d), C (1s), O (1s), Na (1s), Mg (1s), and Ca (1s, 2s, and 2p) orbitals.

According to benchmark calculations carried out by Tecmer et al.[49,66,67] on a series of uranium(VI)-based compounds, the CAM-B3LYP[68] exchange-correlation functional was found to be more accurate than PBE0 for uranyl valence transition energies, for similar optimized structures. Thus, to accurately position the “hot bands”, CAM-B3LYP TD-DFT single-point calculations including spin-orbit coupling (SOC) effects with the ZORA Hamiltonian,[69] and modeling the water solvent with the conductor-like screening model (COSMO) model[70,71,72] were performed at the spin-free ground and excited-state structures, with the Amsterdam Density

Functional package (ADF2018.01).[73] All atoms were described by TZ2P Slater-type basis sets (triple zeta with two polarization functions quality),[74] without the frozen core approximation.

There are controversies in the literature regarding the nature of the "hot band" in the luminescence spectra of uranyl-based complexes.[55] We considered that it corresponds to an average of the lowest-lying electronic transitions, which is a hypothesis difficult to confirm experimentally, but appears reasonable in the case of uranyl compounds. Indeed, at the SOC level, four excited states in the luminescent energy range are very close in energy (within a 900 cm^{-1} range). They correspond to excitations of an electron out from the σ highest occupied molecular orbital (HOMO) into the four non-bonding orbitals noted $f_{-\delta,+\delta}$, $f_{-\phi,+\phi}$, – we refer to orbitals, to ease the chemical discussion, while we should formally refer to spinors – that are nearly degenerate. In the present work the "hot band" is defined after averaging the two pairs among the first four excited states including the Zero-Point-Energy (ZPE) corrections estimated for the ground state and the lowest spin-free triplet excited state, assuming the ZPE being almost identical for all the excited states considered here. The latter assumption is reasonable since the excited states are of similar nature and the previously published theoretical results proved, at least for the symmetric stretches,[60,75] that the excited-state frequencies only vary by few wave numbers (< 10 cm^{-1}).

RESULTS AND DISCUSSIONS

Experimental luminescence spectra. Figure 2 shows the fluorescence spectra acquired with respectively 300 lines mm^{-1} grating for the global emission spectra (a), and 1800 lines mm^{-1} grating for the five specific characteristic peaks (b)-(f) at D = 25 ns. Table 1 lists the aqueous concentrations of alkaline earth metal ions and the speciation calculations results in terms of ternary complexes for each sample solution with published thermodynamic data using PhreeqC,[76] with which the use of SIT (Specific ion Interaction Theory)[77] for modelling the influence of ionic

strength is possible. The sum of [Mg] and [Ca] is maintained at around 0.04 mol kg_w^{-1} for this series with varying ratios of $[Mg^{2+}]/([Ca^{2+}] + [Mg^{2+}])$ from 1 to 0.5.

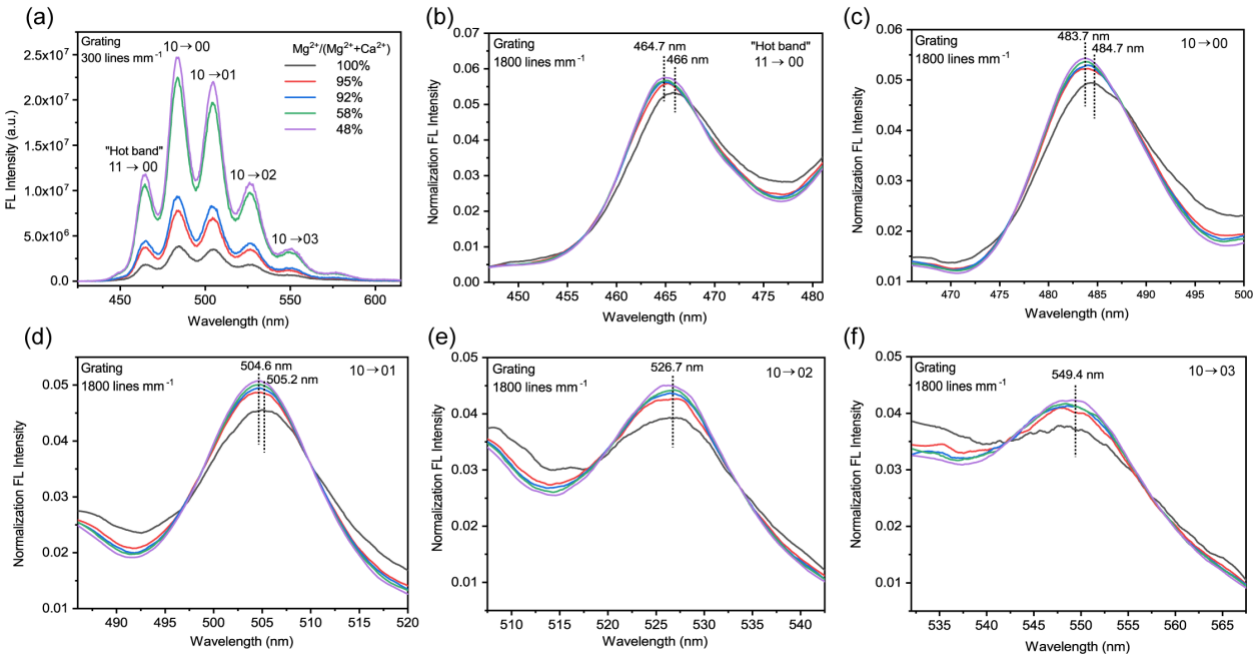

Figure 2. Measured luminescence spectra of U(VI) at various concentration ratios $[Mg^{2+}]/([Mg^{2+}] + [Ca^{2+}])$ using (a) the 300 lines mm^{-1} grating, and (b)-(f) using the 1800 lines mm^{-1} grating for each characteristic peak, normalized to the area of the spectrum in the working wavelength range.

As shown in Figure 2a, the M-U(VI)-CO_3 (M = Mg, Ca) spectra confirm the existence of desirable species. Successive substitution of calcium for magnesium in the ternary triscarbonatouranyl moiety results in markedly enhanced luminescence intensity as the test solutions evolve from the condition where $Mg_nUO_2(CO_3)_3^{(4-2n)-}$ predominate to where $Ca_nUO_2(CO_3)_3^{(4-2n)-}$ are in high proportion (Table 1). The formation constants of Ca complexes are slightly larger than those of Mg complexes. Using reported data,[29] one can express the following equilibrium and complexation constant.

$MgUO_2(CO_3)_3^{2-} + Ca^{2+} = CaUO_2(CO_3)_3^{2-} + Mg^{2+}$ logK = 1.07

This explains that a low quantity of calcium compared to that of magnesium in sample No.2 leads steadily to a relatively large fraction of Ca-UO_2-CO_3 species (49%). On addition of Ca, the increasing luminescence intensity suggests that $Ca_nUO_2(CO_3)_3^{(4-2n)-}$ exhibits higher capacity to fluoresce than $Mg_nUO_2(CO_3)_3^{(4-2n)-}$. Nevertheless, the use of the 300 lines mm^{-1} grating does not allow discriminating the spectral differences since the characteristic peak positions, determined by a Gaussian-based decomposition, differ within the uncertainties among samples. Therefore, the use of the 1800 lines mm^{-1} grating was required to probe the possible differences recorded at ambient temperature.

Table 1 The aqueous compositions of prepared sample solutions calculated with published thermodynamic data from Shang et al[21]., Lee et al.[35] and Dong et al.[29]

No.	$[Ca^{2+}]$ (m)	$CaUO_2(CO_3)_3^{2-}$ (m)	$Ca_2UO_2(CO_3)_3$(aq) (m)	Ca-UO_2-CO_3
1	0	0	0	0%
2	$2.06\ 10^{-3}$	$1.80\ 10^{-5}$	$6.26\ 10^{-6}$	49%
3	$3.16\ 10^{-3}$	$2.09\ 10^{-5}$	$1.15\ 10^{-5}$	65%
4	$1.81\ 10^{-2}$	$1.20\ 10^{-5}$	$3.66\ 10^{-5}$	97%
5	$2.29\ 10^{-2}$	$1.02\ 10^{-5}$	$3.90\ 10^{-5}$	98%
No.	$[Mg^{2+}]$ (m)	$MgUO_2(CO_3)_3^{2-}$ (m)	$Mg_2UO_2(CO_3)_3$(aq) (m)	Mg-UO_2-CO_3
1	$4.30\ 10^{-2}$	$3.72\ 10^{-5}$	$2.07\ 10^{-6}$	79%
2	$3.98\ 10^{-2}$	$1.91\ 10^{-5}$	$9.90\ 10^{-7}$	40%
3	$3.56\ 10^{-2}$	$1.29\ 10^{-5}$	$6.15\ 10^{-7}$	27%
4	$2.52\ 10^{-2}$	$9.09\ 10^{-7}$	$2.95\ 10^{-8}$	2%
5	$2.11\ 10^{-2}$	$5.08\ 10^{-7}$	$1.38\ 10^{-8}$	1%

A closer inspection of Figure 2 b-d shows very small hypsochromic shifts of the first three peaks in the whole spectra when the observed signal evolves from the spectral components from

$Mg_nUO_2(CO_3)_3^{(4-2n)-}$ to those of $Ca_nUO_2(CO_3)_3^{(4-2n)-}$. This could only be detected with the 1800 lines/mm gratings. The observed emission bands at longer wavelengths respond even less sensitively to this evolution of signal. More precisely, the center wavelength of the first peak, *i.e.*, the "hot band", representing the electronic transitions 11→00 undergoes a small shift from 466 nm ($\bar{\nu}$ = 21 459 cm^{-1}) down to 464.7 nm ($\bar{\nu}$ = 21 519 cm^{-1}). The second and the third peaks, corresponding to 10→00 and 10→01, are respectively shifted from 484.7 nm ($\bar{\nu}$ = 20 631 cm^{-1}) down to 483.7 nm ($\bar{\nu}$ = 20 674 cm^{-1}), and from 505.2 nm ($\bar{\nu}$ = 19 794 cm^{-1}) to 504.6 nm ($\bar{\nu}$ = 19 818 cm^{-1}). For the last two peaks — 10→02 and 10→03 (Figure 2 e,f) — the center wavelengths remain nearly invariable. What stands out also in the emission spectra is that the influence of $Mg_nUO_2(CO_3)_3^{(4-2n)-}$ complexes on the center wavelength shift is rather limited once the fraction of Ca complexes is over 50%. As observed in experiments, the hypsochromic shift wavelengths is no longer significant when the fraction of Ca complexes increases from 49% (No.2) to 98% (No.5).

These experimental results first reveal that the interaction of alkaline earth metal ions with triscarbonatouranyl group does not seem to alter the inner-sphere coordination mode of the central uranyl ion in terms of conformational changes, supported by the fact that the emission spectra of M-U(VI)-CO_3 complexes generally display the typical spectral profiles of $UO_2(CO_3)_3^{4-}$ species. Second, only minor modifications in characteristic emission bands have been detected using the 1800 lines mm^{-1} grating when Mg^{2+} is replaced by Ca^{2+} in the ternary species. The most intense peaks of vibronic transitions 10→0ν (ν = 0, 1), as well as the "hot band" are more sensitive to the change of counter ions in the second coordination sphere. The slight bathochromic shifts in the case of Mg (compared to Ca) indirectly give indications that $M^{2+}/UO_2(CO_3)_3^{4-}$ interactions can generate very subtle differences in U(VI) fluorescence behavior where a detailed quantitative

description of the $M^{2+}/UO_2^{2+}/CO_3^{2-}$ system with quantum chemical modelling provides a useful account of the experimental results.

Theoretical ground and excited-state structures. All the key distances for the $M(II)_n,Na(I)_m[UO_2(CO_3)_3]^{(4-m-2n)-}$ are reported in Table 2 along with the experimental data available in literature. To discuss the effect of the second-sphere counter cations on the first coordination shell bond lengths, we take the $Na_3UO_2(CO_3)_3^-$ complex as reference. In its ground-state structure, the following atomic distances were computed: the axial U-O_{ax} bond length at 1.791 Å, the equatorial U-O_{eq} at 2.433 Å, the U-C at 2.902 Å, and the U-O_{dist} (O_{dist} being the most distant oxygen) at 4.141 Å. The U-Na bond distance was equal to 3.823 Å. Our calculated values are in good agreement with EXAFS data obtained in solution.[15,78] One can point out that the use of another functional of the density, namely B3LYP, and slightly different basis sets,[40] has a small impact on the computed distances, as we observe variations not larger than 0.03 Å for the distances within the uranyl first-coordination shell, and 0.14 Å within the second-coordination sphere.

Let us start with general observations on the structural changes induced by the replacement of one Na^+ ion by magnesium or calcium in the second coordination sphere, using the notations of Figure 2. The uranyl subunit, initially linear, was found to be slightly bent, with an O_{ax}-U-O_{ax} angle of about 176°, and all the U-C bond lengths are no longer equivalent because of the different electrostatic interactions (Figure 3). In general, the U-O_{eq} bond lengths with the oxygen atoms closer to the sodium ion (r_1) shortened, whereas the ones with the oxygen atoms closer to the alkaline earth metal (r_3) lengthened; the U-O_{eq} bond lengths (r_2) located between a sodium ion and an alkaline earth ion remained almost unchanged. A similar behavior was obtained for U-C and

$U\text{-}O_{dist}$ bond lengths: they got shorter close to sodium environment (r_A) and longer if magnesium or calcium is near (r_B).

The substitution of one sodium in the reference $Na_3UO_2(CO_3)_3^-$ by one magnesium decreased the $U\text{-}O_{ax}$ bond length by 0.009 Å. The U-C bond lengths vary depending on the counterion present in the vicinity as described previously. In the $Na_2MgUO_2(CO_3)_3$ complex, the computed U-Mg distance is underestimated by our method (about 0.31 Å) as compared to experimental data.[77] The replacement of a second Na^+ by magnesium-induced identical shortening of the $U\text{-}O_{ax}$ bond length as compared to the complex with one magnesium. The U-Mg bond remained the same for both $Na_2MgUO_2(CO_3)_3$ and $NaMg_2UO_2(CO_3)_3^+$ complexes. To the best of our knowledge, the structure of the $Mg_2UO_2(CO_3)_3$ in solution has never been determined experimentally.

By looking at the series of calcium complexes, a similar tendency in the ground state geometries was observed. Like in case of the complex with one calcium, a slightly shorter decrease of axial $U\text{-}O_{ax}$ bond length about 0.006 Å was observed, while the U-C bonds remained essentially unchanged. Unlike the $Na_2MgUO_2(CO_3)_3$ complex, for which U-Na was longer than U-Mg, the U-Ca, and U-Na bonds are found to be almost identical i.e. ~ 3.8 Å in the $Na_2CaUO_2(CO_3)_3$ complex, which is in a good agreement with EXAFS analysis.[15] This elongation of 0.286 Å of the distance to the alkaline earth metal dication is in line with the fact that Mg^{2+} has a smaller ionic radius (0.72 Å) than Ca^{2+} (1.00 Å).[79] The $NaCa_2UO_2(CO_3)_3^+$ complex formed by the addition of a second Ca^{2+} in the outer shell showed that the uranyl unit and first coordination sphere took a similar geometry to that of the $NaMg_2UO_2(CO_3)_3^+$ complex. The difference in U-Mg bond lengths in the complexes with one and two Ca^{2+} ions was found to be 0.061 Å, while the difference in the U-Ca bond lengths was 0.022 Å between the complexes with one and two Ca^{2+} ions.

Looking at the available experimental structures including either Na^+, Ca^{2+} or Mg^{2+}, one can conclude that the U-O_{ax}, U-$O_{carbonate}$ and U-C are rather insensitive with respect to the nature of the cation, and the observed variations when changing the counter cations are of similar magnitude as the ones reported theoretically. Our calculations sometimes underestimate by approximately 0.1 Å at most the distances between the uranium atom and the carbonates ligands and the counter cations. We suspect that this minor structural discrepancy might be imputable to the choice of the functional or to the fact that our chemical model is too limited, as explicit solvent (water molecules) are not included. However, we may assume that our calculated geometries are reliable enough to reproduce trends for the luminescence properties.

Table 2. Ground and excited-state geometries (in Å) of $Na_mM_nUO_2(CO_3)_3^{(4-m-2n)-}$ (M=Mg, Ca; m,n = 0-2) complexes computed with the PBE0 functional in the CPCM water solvent, and compared to selected literature data. The experimental uncertainties are given in parentheses.

	U-O_{ax}	U-O_{eq} (r_1/ r_2/ r_3)	U-C r_A/ r_B	U-O_{dist} r_A/ r_B	U-M	U-Na	Method
Ground state							
$Na_3UO_2(CO_3)_3^-$	1.791	2.433	2.902	4.141		3.823	PBE0/CPCM
	1.806	2.457	2.930	4.188		3.961	B3LYP/PCM[40]
$Na_2MgUO_2(CO_3)_3^-$	1.782	2.387/2.439/ 2.477	2.857/2.9 48	4.089/4. 172	3.515	3.801	PBE0/CPCM
$NaMg_2UO_2(CO_3)_3^+$	1.774	2.390/2.429/ 2.470	2.900/2.9 80	4.119/4. 193	3.511	3.740	PBE0/CPCM
$Na_2CaUO_2(CO_3)_3$	1.785	2.404/2.433/ 2.469	2.874/2.9 31	4.108/4. 162	3.865	3.818	PBE0/CPCM
$NaCa_2UO_2(CO_3)_3^+$	1.779	2.406/2.437/ 2.462	2.902/2.9 53	4.129/4. 176	3.864	3.796	PBE0/CPCM
$UO_2(CO_3)_3^{4-}$	1.81(1)	2.44(1)	2.92(1)	4.17(1)			EXAFS[40]
	1.80(2)	2.44(2)	2.89(2)	4.20(2)			EXAFS[20]

$MgUO_2(CO_3)_3^{2-}$	1.80(1)	2.46(1)	2.91(2)	4.20(2)	3.82(6)		EXAFS[35]
$Na_2CaUO_2(CO_3)_3$	1.79(2)	2.43(2)	2.88(2)	4.15(2)	3.95(2)	3.80(2)	EXAFS[15]
$Ca_2UO_2(CO_3)_3$	1.80(2)	2.43(2)	2.88(2)	4.15(2)	4.05(2)		EXAFS[15]
	1.81(2)	2.44(2)	2.90(2)	4.22(2)	3.94(2)		EXAFS[20]
Excited state		(r_1;r_1'/r_2;r_2'/r_3;r_3')					
$Na_3UO_2(CO_3)_3^-$	1.826	2.442	2.908	4.147		3.822	TD-PBE0/CPCM
$Na_2MgUO_2(CO_3)_3^-$	1.817	2.374/2.410/ 2.436/ 2.447/2.482/ 2.505	2.857/ 2.952/2.958	4.090/4.180/4.183	3.521	3.783/ 3.809	TD-PBE0/CPCM
$NaMg_2UO_2(CO_3)_3^+$	1.810	2.379/2.380/ 2.454/ 2.455/2.479/ 2.480	2.903(x2) /2.988	4.123/4.124/4.202	3.518/3.519	3.717	TD-PBE0/CPCM
$Na_2CaUO_2(CO_3)_3$	1.820	2.406/2.422/ 2.425/ 2.428/2.482/ 2.497	2.882/2.933/2.927	4.118/4.164/ 4.168	3.875	3.817/ 3.806	TD-PBE0/CPCM
$NaCa_2UO_2(CO_3)_3^+$	1.815	2.398(x2)/2.462(x2)/2.467(x2)	2.908(x2) /2.956	4.135(x2)/4.180	3.871(X2)	3.778	TD-PBE0/CPCM

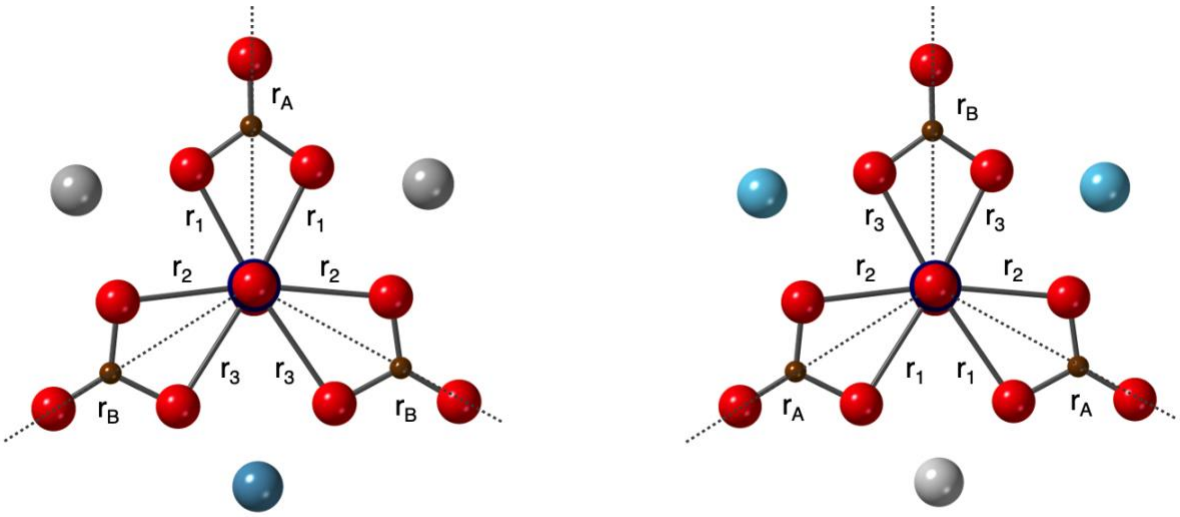

Figure 3. Schematic notation of U-CO_3 bonds in a) $Na_2MUO_2(CO_3)_3$ and b) $NaM_2UO_2(CO_3)_3^+$(M = Mg, Ca) complexes depending on the position of the alkaline earth metals in the second coordination sphere. Notation r_1, r_2 and r_3 correspond to different U-O_{eq} bonds, while the dashed lines r_A and r_B correspond to different U-C and U-O_{dist} bonds. In red - O, brown - C, dark blue - U, gray - Na, light blue - Ca, Mg.

The bond lengths of the excited-state structures are reported in Table 2, and are compared to the bond lengths found in the ground-state geometries. For the reference $Na_3UO_2(CO_3)_3^-$ complex and both series of magnesium and calcium complexes, the U-O_{ax} bond elongates by 0.035-0.036 Å upon excitation. One can see that for the Mg/Ca systems, the bond lengths of the U-O_{eq} are not degenerate any longer. An increase of the U-O_{eq}, U-C and U-O_{dist} bonds between the ground and excited states was found to be in the range from 0 to 0.01 Å. The positions of Na^+ and alkaline earth cations in the excited state were found to be rather similar after excitation of an electron. The U-Na bond lengths shortened by up to 0.023 Å along the series, while the excitation process resulted in a small elongation of the U-M bond by at most 0.01 Å. Additional analyses of the

structural changes are presented in a table form in the ESI. As there is no literature data available for the excited state structures of triscarbonatouranyl complexes, it is difficult to quantitatively estimate the accuracy of the TD-DFT relaxed calculations. Nevertheless, small elongations of atomic bonds were observed as could be expected as a result of the transition from bonding to non-bonding orbital of the uranium, as observed for the uranyl tetrahalide complexes.[50] As the main objective here is to describe the evolution of the luminescence properties in the series, the methodology appears to be trustworthy.

The intensity distributions observed in the luminescence spectra of U(VI)-based complexes are closely related to the uranyl vibrational modes, mostly the uranyl symmetrical stretching ν_s. Thus, we have reported in Table 3 the computed frequency values of the ground and excited state uranyl bending ν_b, symmetrical ν_s and anti-symmetrical ν_a stretching modes.

The values for ν_s and ν_a in the $K_4UO_2(CO_3)_3$ crystal were measured by Raman and IR spectroscopies at 300 K.[8080] The experimental solid-state symmetrical and anti-symmetrical stretching frequencies amounted to 812 and 889 cm^{-1}, and agreed well with ours, 837 and 877 cm^{-1}, computed for the $Na_3UO_2(CO_3)_3^-$ complex with inclusion of long-range hydration effects. The ν_b for this complex was computed at 286 cm^{-1} but it could not be compared to any experimental data. It is noteworthy that with the addition of counterions, the uranyl bending motion is coupled with the libration and deformation motions of the carbonate ligands. It is thus inappropriate to discuss this vibrational frequency as pure bending mode of the uranyl unit. The same observation was made by Kalashnyk et al. for the andersonite mineral $Na_2CaUO_2(CO_3)_3 \cdot xH_2O$ (x=5.3 – 5.6)[42] for which they reported ν_b in the 225-285 cm^{-1} range. We calculated 255-282 cm^{-1} for the $Na_2CaUO_2(CO_3)_3$ complex, which appears to be consistent. Moreover, as the charge of the complex increases with the addition of Mg^{2+} or Ca^{2+} in the second coordination sphere, gradual

shifts to larger vibrational energies of the uranyl stretching modes ν_s and ν_a were observed when sodium was replaced by alkaline earth metal, with a shift of about +17-21 cm^{-1} for the magnesium complexes, and +13-14 cm^{-1} for the calcium complexes.

Table 3 Ground and excited-state vibrational frequencies (in cm^{-1}) of $Na_mM_nUO_2(CO_3)_3^{(4-m-2n)-}$ (M=Mg, Ca; m,n = 0-2) complexes computed with the PBE0 functional in the CPCM water solvent.

	ν_b	ν_s	ν_a	Method
Ground state				
$Na_3UO_2(CO_3)_3^-$	286	837	877	PBE0/CPCM
$Na_2MgUO_2(CO_3)_3$	230-285	857	898	PBE0/CPCM
$NaMg_2UO_2(CO_3)_3^+$	250-305	874	918	PBE0/CPCM
$Na_2CaUO_2(CO_3)_3$	255-282	850	891	PBE0/CPCM
$NaCa_2UO_2(CO_3)_3^+$	242-288	862	905	PBE0/CPCM
$K_4UO_2(CO_3)_3$		806	882	IR/Raman[80]
$Na_2CaUO_2(CO_3)_3$,$x$$H_2O$ (x=5.3 – 5.6)	225-285	833	931	Raman[42]
Excited state				
$Na_3UO_2(CO_3)_3^-$	276	712	777	TD-PBE0/CPCM
$Na_2MgUO_2(CO_3)_3^-$	238-278	722	796	TD-PBE0/CPCM
$NaMg_2UO_2(CO_3)_3^+$	224-307	739	812	TD-PBE0/CPCM
$Na_2CaUO_2(CO_3)_3$	228-275	720	791	TD-PBE0/CPCM
$NaCa_2UO_2(CO_3)_3^+$	233-278	728	801	TD-PBE0/CPCM

In the first excited state, the uranyl vibrational stretching frequencies are smaller than in the ground state whereas the bending ones are nearly identical. For the reference $Na_3UO_2(CO_3)_3^-$ complex, symmetrical and anti-symmetrical stretching modes decreased by 125 and 100 cm^{-1}, respectively. A similar tendency, within 10 cm^{-1}, was observed for the other $Na_mM_nUO_2(CO_3)_3^{(4-}$

$^{m-2n)-}$ (M = Mg, Ca; m,n = 0-2) compounds. A complete analysis of vibrational frequencies behavior is available in the ESI.

Experimental and theoretical emission energies. In experimental luminescence spectra the first observed electronic transition, usually called the "hot band" is located near 465 nm, and can be detected at room temperature.[13] The study of the electronic structure of uranyl-based complexes shows that the luminescent state usually corresponds to the first low-lying triplet states that are nearly degenerate. Even though the triplet-singlet transitions are forbidden by the spin selection rule in the spin-orbit free picture, this rule is relaxed in the intermediate coupling scheme when spin-orbit coupling is accounted for and can be observed experimentally. The analysis of the molecular orbitals involved in excitations to the first four triplet states (1a-4a) confirmed that uranyl luminescence originates from transitions involving an electron placed in one of the four non-bonding 5f orbitals of uranium(VI) to an orbital that has a uranyl σ (5f, 6d) character mixed with the 2p atomic orbitals of the carbonate oxygens (Figure 4). Thus, the emission process in the triscarbonatouranyl bidentate complexes corresponds to a local transition from one of the non-bonding to bonding uranyl orbitals, with a moderate metal-to-ligand charge transfer character.

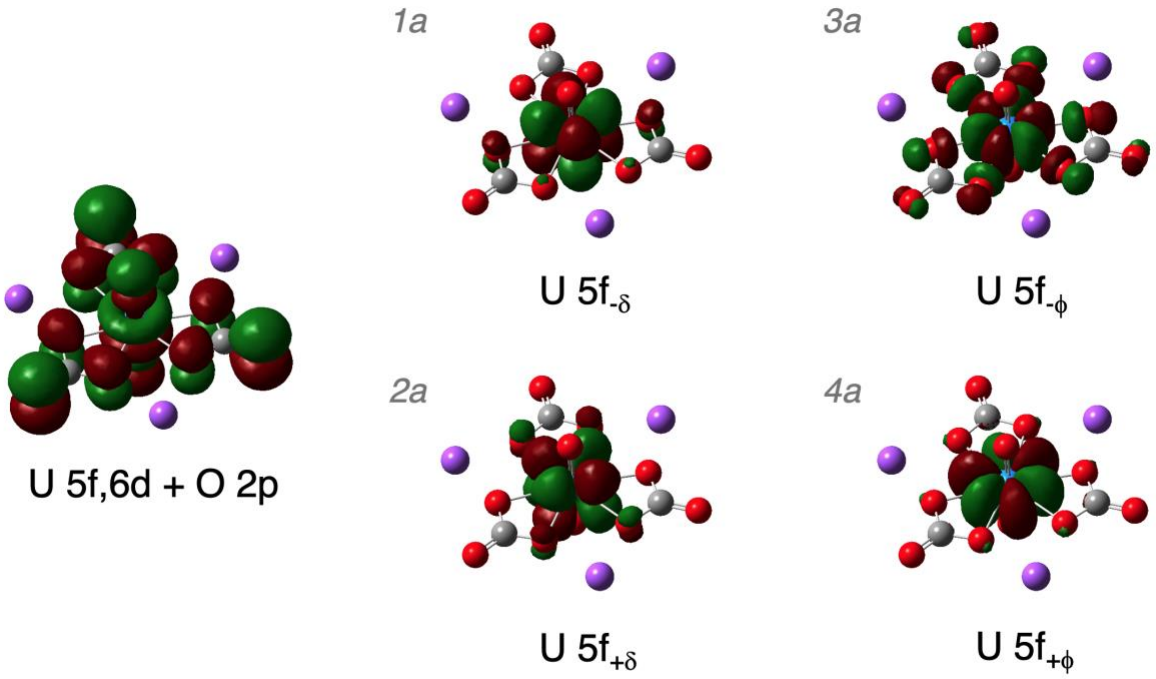

Figure 4. The highest occupied and lowest unoccupied molecular orbitals of $Na_3UO_2(CO_3)_3^-$ involved in the triplet-singlet electronic transitions, responsible of uranyl luminescence. The molecular orbitals were computed at the gas phase ground-state structure at the DFT/PBE0 level of theory.

The origin of the spectral envelope usually shifts along the energy scale as a function of the nature of the equatorial ligands, the stoichiometry and the complex structure. Several spectroscopic studies evidenced a luminescence blue shift of the carbonate complexes as compared to many other uranyl species such as phosphates, halides or hydrates.[20,31,34,13] From previous studies on triscarbonatouranyl complexes[8,35], the blue shift was estimated to 7, 15, and 25 nm (in approximately 300 - 1100 cm^{-1}) with respect to $UO_2(H_2O)_5^{2+}$, $UO_2Cl_4^{2-}$ and $UO_2(NO_3)_2$ complexes, respectively. Wang et al.[13] inferred that ionic interactions between the uranyl ion and anions with stronger basicity lead to larger decrease of the symmetric O=U=O stretching

frequency, along with a larger redshift of the luminescence spectra. This explanation holds for carbonate ligands that are softer bases than chlorides, for instance.[81]

Theoretically, the vertical emission energy, averaged by their nature $E_{1a,2a}$ and $E_{3a,4a}$ should explain the position of the "hot band." The theoretical $E_{1a,2a}$ and $E_{3a,4a}$ values together with the experimental emission maxima are shown in Table 4. The experimental "hot band" values for the series of magnesium and calcium triscarbonatouranyl complexes agreed well with the previous spectroscopic studies[8,35] and usually remain constant within 2 nm. In aqueous solution, Mg^{2+} exhibits a stronger polarizing effect than Ca^{2+} due to its higher charge density. When M^{2+} counterions interact with $UO_2(CO_3)_3^{4-}$, the global electron density of the negative ion group, especially of the equatorial oxygen atoms in carbonates, would be more distorted towards the Mg^{2+} than Ca^{2+}. The effect of distortion could change the bonding character from ionic to covalent if enough valence electrons are attracted to the positive ions.[82] The electronic redistribution occurred in Mg-UO_2-CO_3 complexes results in a less symmetric structure, which probably reasons out the weak shift of emission spectra to longer wavelengths. In a previous study, the effect of molecular symmetry on fluorescence results has been specially studied by comparing the experimental parameters of a set of organic molecules.[83] It was shown that the more symmetric molecules often give rise to larger quantum yield and longer decay time because of several transitions forbidden by symmetry. For the more symmetric Ca-UO_2-CO_3 complexes, the decrease in the number of non-radiative pathways theoretically contributes to less energy losses between excitation and emission, thus should cause the hypsochromic shift in emission spectra.[84]

Table 4 Experimental and computed "hot band" energies (in nm and cm^{-1}) of $Na_mM_nUO_2(CO_3)_3^{(4-m-2n)-}$ (M=Mg, Ca; m,n = 0-2) complexes in water. Theoretical values were obtained at all-electron SOC CAM-B3LYP level of theory, modeling the water solvent with the COSMO model.

	Exp.		$E_{1a,2a}$[a]		$E_{3a,4a}$[a]	
	nm	cm^{-1}	nm	cm^{-1}	nm	cm^{-1}
Mg-UO_2-CO_3	464.7[b]/ 466[8]	21552/ 21459				
Ca-UO_2-CO_3	466[b]/ 467[35]	21459/ 21413				
$Na_3UO_2(CO_3)_3^-$			487	20543	467	21412
$Na_2MgUO_2(CO_3)_3$			492	20339	473	21131
$NaMg_2UO_2(CO_3)_3^+$			491	20372	474	21111
$Na_2CaUO_2(CO_3)_3$			491	20362	473	21421
$NaCa_2UO_2(CO_3)_3^+$			493	20268	476	21211
$UO_2(H_2O)_5^{2+}$	471[85]	21231				
$[A336]_2[UO_2Cl_4]$[c],[d]	479[50]	20877	499	20044	485	20599
$UO_2(NO_3)_2{\cdot}2H_2O$[d]	490[86]	20408	494	20260	484	20651

[a] the reported $E_{1a,2a}$ and $E_{3a,4a}$ values correspond to the average of the two first pairs of vertical emission energies (See Figure 4, see ESI) computed at the lowest triplet state geometries, with addition of the zero-point energy corrections of the ground and first excited states; [b] this work; [c] in *n*-dodecane; [d] $E_{1a,2a}$ and $E_{3a,4a}$ values were obtained at TD-DFT/PBE0 level of theory in the corresponding media

The comparison of the $E_{1a,2a}$ and $E_{3a,4a}$ theoretical energies showed that the $E_{3a,4a}$ values agree better with experimental "hot band" values than the $E_{1a,2a}$. However, the $E_{1a,2a}$ energies are in the range of the triscarbonatouranyl spectral envelope, thus they can contribute to the experimental

spectra. For the Mg^{2+} and Ca^{2+} triscarbonatouranyl complexes our calculations showed a redshift from $Na_3UO_2(CO_3)_3^-$ to $Na_2MUO_2(CO_3)_3$ and $NaM_2UO_2(CO_3)_3^+$ as a result of negative and positive charges in our model structures used for calculations, while the complexes in solution are stabilized by counter-ions present in the working solution. It is worth noting that our calculations did not show any significant impact of the alkaline earth metal on the position of the emission maxima. It is still difficult to predict emission energies of actinides with a high precision, but our method allowed to reproduce accurately the blue shift of a luminescence profile of triscarbonatouranyl complexes. As compared to similar calculations of the $E_{3a,4a}$ performed in our group at the same level of theory for the $[A336]_2[UO_2Cl_4]$ in *n*-dodecane and $UO_2(NO_3)_2{\cdot}2H_2O$ in water media, our method is qualified to reproduce experimental "hot band" position within ±10 nm (~500 cm^{-1}) accuracy.

Vibronic progressions. The luminescence spectrum of U(VI) complexes typically shows well-spaced vibronic progressions that overlap with the pure electronic transition originates from the luminescent state to the ground state. The vibronic progression means that there is a coupling to symmetrical stretching mode of uranyl unit during the emission process. The theoretical and experimental luminescence spectra of Mg^{2+} and Ca^{2+} triscarbonatouranyl complexes are shown in Fig. 5. The theoretical spectra were all shifted to the position of the experimental "hot band" for the sake of spectra comparison. The calculated spectrum of $Na_3UO_2(CO_3)_3^-$ was not reported because it was considered not reliable due to the geometrical distortion of some electron configurations leading to a deficiency of degeneracy.

The intensity of luminescence depends on the quantum yield, which is basically a ratio of the rate of de-excitation by photons emission to the rate of de-excitation by both radiative and non-radiative processes. It is usually much lower than unity for uranyl species since non-radiative

transitions are the major part of relaxation of the excited molecules.[55] This is why the prediction of real experimental intensities from quantum chemical model is necessarily incomplete, and only relative peak intensities and trends are relevant.

For all the triscarbonatouranyl complexes the vibronic part starts at the 10→00 transition with the band spacing equal to the ground state uranyl stretching frequency ν_s^{GS}, while the 11→00 "hot band" appears at higher energy from the 10→00 transition. The analysis of $E_{1a,2a}$ and $E_{3a,4a}$ theoretical emission energies has showed that the $E_{1a,2a}$ agreed well with the experimental 10→00 transition, while $E_{3a,4a}$ is much closer to the 11→00 value and spaced from $E_{1a,2a}$ by a ν value ranging from 729 to 798 cm^{-1} (See Table 2). Such observation is supporting the possibility of the simultaneous contributions of two excited states to the spectrum. Thus, it has been assumed that there are two vibronic progressions starting at $E_{1a,2a}$ and $E_{3a,4a}$ energies and contributing to the 10→00 and 11→00 transitions, respectively. To reconstruct theoretical spectra, two vibronic progressions, computed out of the first low-lying excited state, were superimposed on the same energy scale.

The analysis of computed spectra showed no other significant contributions than uranyl symmetrical stretching mode, which means that the coupling scheme remains the same for Mg^{2+} and Ca^{2+} triscarbonatouranyl complexes. The detailed assignment of the peaks is provided in the ESI. The experimental and theoretical spectral characteristics such as positions of the peaks and the band-spacing values are reported in Table 5.

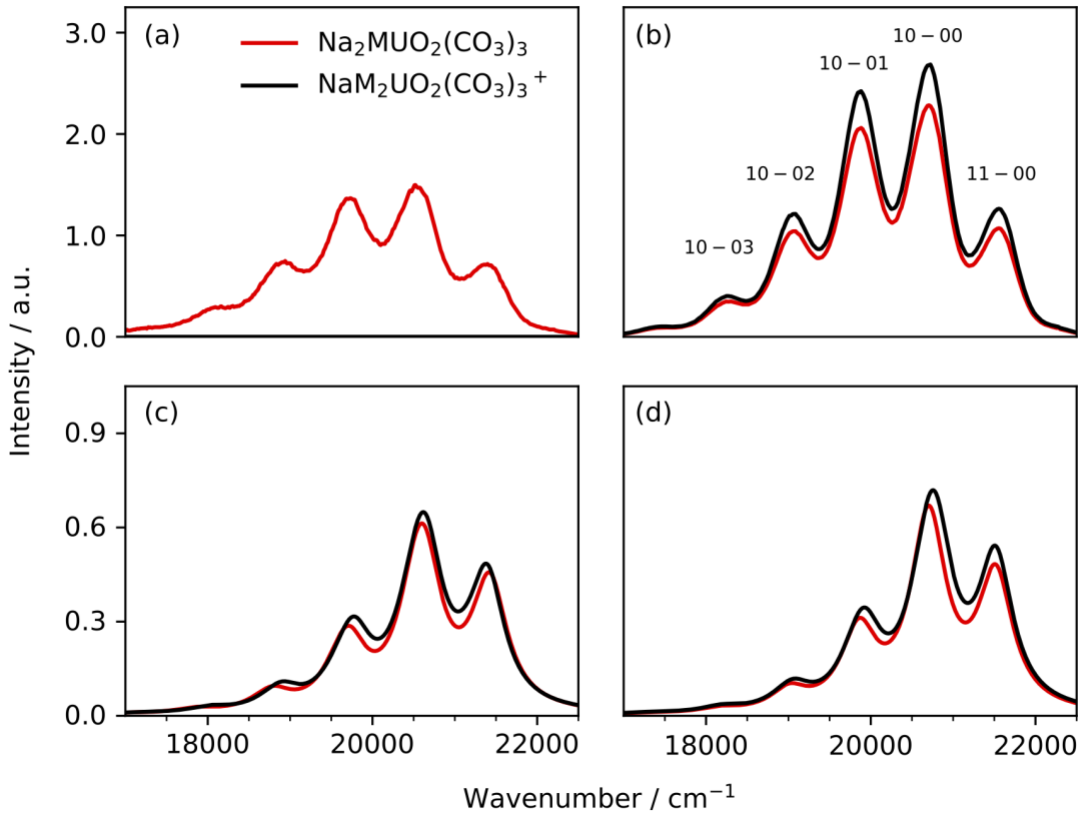

Figure 5. Deconvoluted experimental spectra of (a) $MgUO_2(CO_3)_3^{2-}$, and (b) $CaUO_2(CO_3)_3^{2-}$ and $Ca_2UO_2(CO_3)_3$ from TRLFS measurements. Theoretical luminescence spectra in water of (c) $Na_2MgUO_2(CO_3)_3$ (reconstructed as described in ESI) and $NaMg_2UO_2(CO_3)_3^+$, and (d) $Na_2CaUO_2(CO_3)_3$ and $NaCa_2UO_2(CO_3)_3^+$.

The peak positions were predicted with the maximal deviation of about 224 cm^{-1} for Mg^{2+} and 131 cm^{-1} for Ca^{2+} complexes. Theoretical values of the band spacing are overestimated by maximum 48 and 30 cm^{-1} for Mg^{2+} and Ca^{2+} systems, respectively, compared to experimentally obtained values. The calculated ν values are found to be systematically lower by about 100 cm^{-1} with respect to experimental data, what is deduced from the spacing between the 11→00 and 10

→00 transitions, and they are very similar to the excited state symmetrical stretching mode. The higher values attributed to ν from experimental spectra could originate from small additional contributions to the vibronic coupling that are not accounted for. Indeed, our theoretical model does not account for explicit water molecules in the structure's calculations, and anharmonicity effects were not accounted for in the spectra computations. Although the model could be improved, but with additional calculation cost, we conclude that the agreement between the peak positions in the experimental and computed spectra is satisfactory for such modelling of luminescence peaks from the uranyl complexes.

Table 2. Experimental and theoretical spectral characteristics of triscarbonatouranyl complexes. Experimental ν_s^{GS} and ν values were obtained by Lorentzian fitting procedure.

Complex	Spectral maxima (cm^{-1})					ν_s^{GS}[a] (cm^{-1})	ν [b] (cm^{-1})
	11→00	10→00	10→01	10→02	10→03		
Experimental							
Mg-UO_2-CO_3	21459	20631	19794	18986	18202	826	828
Ca-UO_2-CO_3	21519	20674	19818	18986	18202	832	845
Theoretical							
$Na_2MgUO_2(CO_3)_3$	21459[c]	20737	19822	18904	17978	857	792
$NaMg_2UO_2(CO_3)_3^+$	21459[c]	20720	19847	18972	18099	874	739
$Na_2CaUO_2(CO_3)_3$	21519[d]	20799	19949	19099	18249	850	798
$NaCa_2UO_2(CO_3)_3^+$	21519[d]	20790	19928	19066	18205	862	729

[a,b] The ν_s^{GS} corresponds to the averaged band-spacing values between vibronic transitions, the ν corresponds to spacing between the 11→00 and 10→00 transitions. The spectral characteristics in nm is available in the Tables S8 and S9 of ESI; [c,d] the 11→00 was taken from experimental Mg-UO_2-CO_3 and Ca-UO_2-CO_3 emission spectra to match position of theoretical peaks with experimental ones

It is worth analyzing the change of the theoretical and experimental luminescence intensities of the complexes not in absolute terms but relative ones for the two alkaline earth metal ions. First, the comparison of theoretical intensities of Mg^{2+} and Ca^{2+} complexes between each other is scientifically wrong because the used theoretical models do not account for many other experimental factors that have an influence on luminescence intensities (pH, ionic strength etc.). Moreover, experimental luminescence intensities of the whole spectral envelope depend on additional factors like the effective laser excitation of each species, influence of experimental apparatus such as slot width, or quenching effects, which are not included in the theoretical calculations.

The spectrum of the $Mg_2UO_2(CO_3)_3$ complex was fully calculated whereas we were unsuccessful in calculating the vibronic progressions in $Na_2MgUO_2(CO_3)_3$ in the framework of the Franck-Condon harmonic approximation. Indeed, we observed a distortion of the $UO_2(CO_3)_3^{4-}$ moiety upon Mg^{2+} complexation in $Na_2MgUO_2(CO_3)_3$, that was reflected in the out-of-plane molecule distortion caused by increasing of a polarizing effect of Mg^{2+} in water. The full theoretical spectrum of $Na_2MgUO_2(CO_3)_3$ could be obtained using gas-phase geometries of $Na_2MgUO_2(CO_3)_3$ including water structures corrections, and then plotted in Fig 5c. The detailed procedure of a spectrum prediction is available in the ESI.

On Fig 5c the calculated intensity of the 10→01 peak in the magnesium complexes, decreases more than the experimental Mg-UO_2-CO_3 intensity because the calculations might underestimate the theoretical U-O_{ax} bond length changes upon excitation. From Table S3 in ESI we observed that U-O_{ax} bond displacement from the ground to the luminescent state is identical and equal to 0.036 Å. Thus, our theoretical model showed that even if the $Mg_2UO_2(CO_3)_3$ could form in experimental conditions, its luminescence spectrum will be hardly distinguished by TRLFS from the one by

$MgUO_2(CO_3)_3$, except if they have significantly different luminescence lifetimes. On the contrary, the addition of a second Ca^{2+} ion to the triscarbonatouranyl complexes induced an enhancement of the experimental luminescence intensities (Fig. 5b), as shown otherwise.[8,21,78] This enhancement was well reproduced in the computed spectra comparing the $Na_2CaUO_2(CO_3)_3$ and $NaCa_2UO_2(CO_3)_3^+$ model systems (Fig. 5d). This result is consistent with the fact that the U-O_{ax} bond changes are slightly different and equal to 0.035 and 0.036 Å for complexes with one and two Ca^{2+}, respectively.

The theoretical results confirmed that the luminescence intensities of the triscarbonatouranyl complexes depend on the structure of uranyl unit with a major contribution from the U-O_{ax} bond displacement, and only a minor one from equatorial ligands. The intensity trends of the 10→00 transition were correctly reproduced by the quantum chemical simulations without any fitting.

CONCLUSIONS

The interaction of the triscarbonatouranyl complex $UO_2(CO_3)_3^{4-}$ with alkaline earth metal ions M^{2+} (Mg and Ca) in solution is known to induce stable complex of stoichiometry $M_nUO_2(CO_3)_3^{(4-2n)-}$ (n=1, 2), which has important implication on uranyl speciation in different environments. These species have specific luminescence features, as a result of the electronic configurations of the ground and excited states, the vibronic states and vibrational coupling. The luminescence of the complexes with Mg^{2+} (n=1) and Ca^{2+} (n=1, 2) were measured by TRLFS and compared for the first time with simulated spectra obtained using quantum mechanics applied to model structures $Na_mM_nUO_2(CO_3)_3^{(4-m-2n)-}$ (M = Mg, Ca; m, n = 0-2). The ground and excited state geometries of each structure were optimized by DFT/PBE0 and TD-DFT/PBE0 at the spin-free level including relativistic effects and water solvent effects (CPCM). The first low-lying excited states were successfully computed together with the vibrational harmonic frequencies for $Na_2MgUO_2(CO_3)_3$,

$NaMg_2UO_2(CO_3)_3^+$, $Na_2CaUO_2(CO_3)_3$, and $NaCa_2UO_2(CO_3)_3^+$. The 11→00 "hot band" positions were determined by the more accurate TD-DFT/CAM-B3LYP with single-point calculations. This theoretical approach enabled to calculate the main luminescence emissions of the complexes with the corresponding assignment of the electronic transitions and vibronic modes involved. The resulting calculated spectra showed a very good agreement with experimental band positions and band spacing attributed to $MgUO_2(CO_3)_3^{2-}$, $CaUO_2(CO_3)_3^{2-}$, and $Ca_2UO_2(CO_3)_3$. Particularly, the calculations reproduce fairly well the blue shift of the triscarbonatouranyl complexes luminescence as compared with other uranyl complexes. The calculations also confirmed the similarities of the spectra for Mg^{2+} and Ca^{2+} complexes, and correctly reproduced the increase of the luminescence intensity upon addition of a second Ca^{2+} as a result of a slightly large increase of the $U\text{-}O_{ax}$ distance upon excitation and change of polarizing effect. In the case of Mg^{2+} complexes, the $U\text{-}O_{ax}$ bond change was found to be the same for both $Na_2MgUO_2(CO_3)_3$ and $Mg_2UO_2(CO_3)_3$, the polarizing effect of magnesium is found to have more impact on the $U\text{-}O_{yl}$ unit, suggesting that the luminescence of these complexes would hardly be distinguished experimentally, unless they are showing very different decay times.

The QM method applied in this work offered an appropriate compromise between the calculation cost and the accuracy of the results in comparison with experimental data. Further works could improve the representativity of the model structures by adding explicit water molecules in the structures for instance that will affect the positions of the alkaline earth metal ions and vibronic coupling.

ASSOCIATED CONTENT

Supporting Information

The following file supplemental-uo2co3.pdf is available free of charge. It contains:

Extraction of the pure spectra of the (Mg/Ca–) UO_2−CO_3) species from the raw TRLFS data; procedure to estimate the spectrum of the $Na_2MgUO_2(CO_3)_3$ complex in water; assignments for theoretical spectra. An independent ZIP file contains the Cartesian coordinates of all calculated structures.

AUTHOR INFORMATION

Corresponding Authors

Thomas Vercouter – DEN-Service d'Etudes Analytiques et de Réactivité des Surfaces (SEARS), CEA, Université Paris-Saclay, F-91191 Gif-sur-Yvette, France ; http://orcid.org/0000-0002-5315-0251; Email :thomas.vercouter@cea.fr

Valérie Vallet - Université de Lille, CNRS, UMR 8523 – PhLAM – Physique des Lasers Atomes et Molécules, F-59000 Lille, France ; http://orcid.org/0000-0002-2202-3858; Email :valerie.vallet@univ-lille.fr

ACKNOWLEDGMENT

We acknowledge support by the French government through the Program "Investissement d'avenir" (LABEX CaPPA/ANR- 11-LABX-0005-01 and I-SITE ULNE/ANR-16-IDEX-0004 ULNE), as well as by the Ministry of Higher Education and Research, Hauts de France council and European Regional Development Fund (ERDF) through the Contrat de Projets État-Région (CPER CLIMIBIO). Furthermore, this work was granted access to the HPC resources of CINES/IDRIS/TGCC under the allocation 2019−2020 (A0070801859) made by GENCI. We also acknowledge the CEA for the Ph.D. grant given to H.O.

SYNOPSYS

Luminescence spectra of $Na_2MgUO_2(CO_3)_3$, $NaMg_2UO_2(CO_3)_3^+$, $Na_2CaUO_2(CO_3)_3$, and $NaCa_2UO_2(CO_3)_3^+$ were computed with ab initio methods including long-range water solvation effect. The evolution of theoretical intensities is in a good agreement with the recorded experimental luminescence spectra obtained by time-resolved laser-induced fluorescence spectroscopy (TRLFS) in aqueous phase. The analysis of the theoretical results reveals the importance of alkali earth-counter cations' polarizing effect as well as their influence on the structures and luminescence intensities.

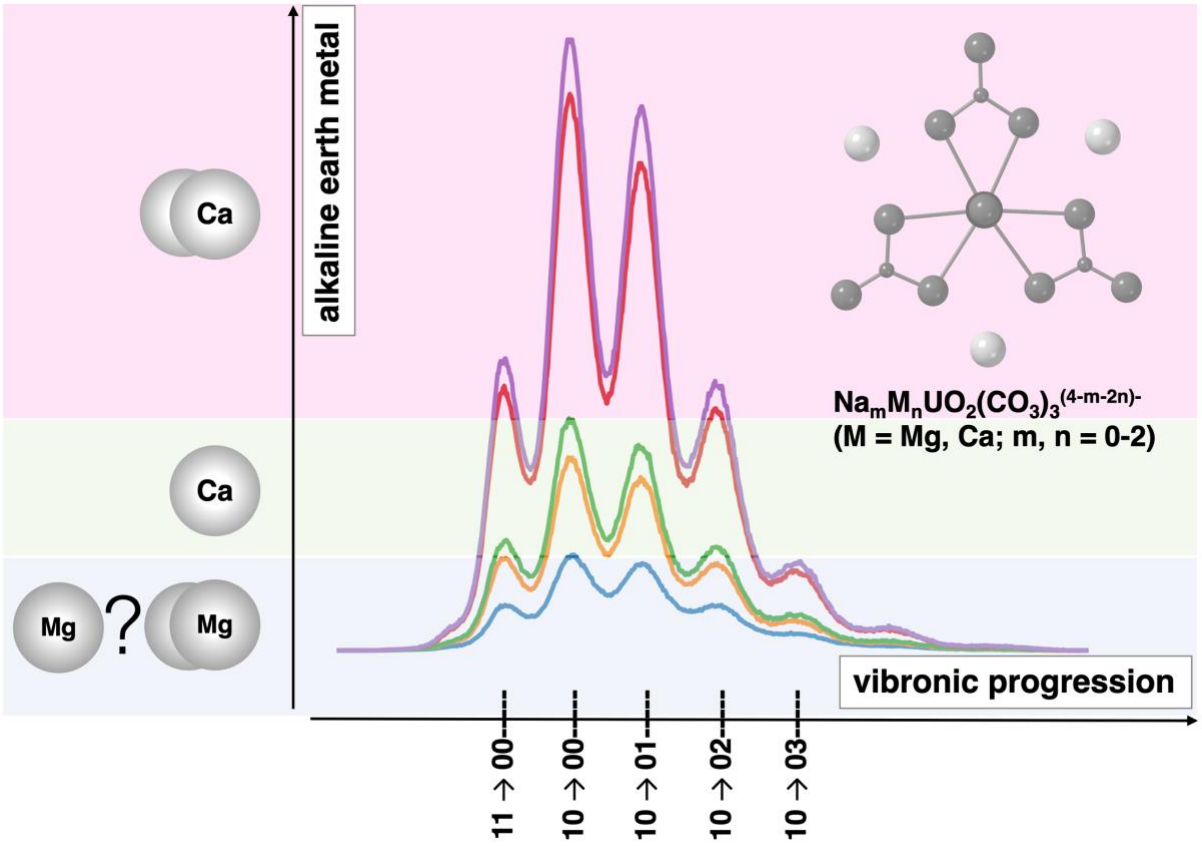

Figure TOC. For Table of Contents Only

REFERENCES

(1) Moulin, C.; Decambox, P.; Moulin, V.; Decaillon, J. G. Uranium Speciation in Solution by Time-Resolved Laser-Induced Fluorescence. *Anal. Chem.* **1995**, *67* (2), 348–353. https://doi.org/10.1021/ac00098a019.

(2) Moulin, C.; Laszak, I.; Moulin, V.; Tondre, C. Time-Resolved Laser-Induced Fluorescence as a Unique Tool for Low-Level Uranium Speciation. *Appl. Spectrosc.* **1998**, *52* (4), 528–535. https://doi.org/10.1366/0003702981944076.

(3) Eliet, V.; Bidoglio, G.; Omenetto, N.; Parma, L.; Grenthe, I. Characterization of Hydroxide Complexes of Uranium(VI) by Time-Resolved Fluorescence Spectroscopy. *J. Chem. Soc. Trans.* **1995**, *91* (15), 2275–2285. https://doi.org/10.1039/FT9959102275.

(4) Meinrath, G.; Lis, S.; Stryla, Z.; Noubactep, C. Lifetime and Fluorescence Quantum Yield of Uranium(VI) Species in Hydrolyzed Solutions. *J. Alloys Compd.* **2000**, *300*, 107–112. https://doi.org/10.1016/S0925-8388(99)00739-2.

(5) Moll, H.; Geipel, G.; Brendler, V.; Bernhard, G.; Nitsche, H. Interaction of Uranium(VI) with Silicic Acid in Aqueous Solutions Studied by Time-Resolved Laser-Induced Fluorescence Spectroscopy (TRLFS). *J. Alloys Compd.* **1998**, *271*, 765–768. https://doi.org/10.1016/S0925-8388(98)00203-5.

(6) Couston, L.; Pouyat, D.; Moulin, C.; Decambox, P. Speciation of Uranyl Species in Nitric-Acid Medium by Time-Resolved Laser-Induced Fluorescence. *Appl. Spectrosc.* **1995**, *49* (3), 349–353. https://doi.org/10.1366/0003702953963553.

(7) Geipel, G.; Brachmann, A.; Brendler, V.; Bernhard, G.; Nitsche, H. Uranium(VI) Sulfate

Complexation Studied by Time-Resolved Laser-Induced Fluorescence Spectroscopy (TRLFS). *Radiochim. Acta* **1996**, *75* (4), 199–204. https://doi.org/10.1524/ract.1996.75.4.199.

(8) Lee, J. Y.; Yun, J. Il. Formation of Ternary $CaUO_2(CO_3)_3^{2-}$ and $Ca_2UO_2(CO_3)_3(Aq)$ Complexes under Neutral to Weakly Alkaline Conditions. *Dalton Trans.* **2013**, *42* (27), 9862–9869. https://doi.org/10.1039/c3dt50863c.

(9) Vercouter, T.; Vitorge, P.; Amekraz, B.; Moulin, C. Stoichiometries and Thermodynamic Stabilities for Aqueous Sulfate Complexes of U(VI). *Inorg. Chem.* **2008**, *47* (6), 2180–2189. https://doi.org/10.1021/ic701379q.

(10) Geipel, G.; Bernhard, G.; Rutsch, M.; Brendler, V.; Nitsche, H. Spectroscopic Properties of Uranium(VI) Minerals Studied by Time-Resolved Laser-Induced Fluorescence Spectroscopy (TRLFS). *Radiochim. Acta* **2000**, *88*, 757--762. https://doi.org/10.1524/ract.2000.88.9-11.757.

(11) Lehmann, S.; Geipel, G.; Foerstendorf, H.; Bernhard, G. Syntheses and Spectroscopic Characterization of Uranium(VI) Silicate Minerals. *J. Radioanal. Nucl. Chem.* **2008**, *275* (3), 633–642. https://doi.org/10.1007/s10967-007-7060-z.

(12) Massuyeau, F.; Perry, D. L.; Kalashnyk, N.; Faulques, E. Spectroscopic Markers for Uranium(VI) Phosphates. Part II: The Use of Time-Resolved Photoluminescence. *RSC Adv.* **2017**, *7* (2), 919–926. https://doi.org/10.1039/c6ra26157d.

(13) Wang, Z.; M. Zachara, J.; Liu, C.; Gassman, P.; R. Felmy, A.; B. Clark, S. A Cryogenic Fluorescence Spectroscopic Study of Uranyl Carbonate, Phosphate and Oxyhydroxide

Minerals. *Radiochim. Acta* **2008**, *96*, 591–598. https://doi.org/10.1524/ract.2008.1541.

(14) Amayri, S.; Arnold, T.; Reich, T.; Foerstendorf, H.; Geipel, G.; Bernhard, G.; Massanek, A. Spectroscopic Characterization of the Uranium Carbonate Andersonite $Na_2Ca[UO_2(CO_3)_3]\cdot 6H_2O$. *Environ. Sci. Technol.* **2004**, *38* (22), 6032–6036. https://doi.org/10.1021/es049417l.

(15) Amayri, S.; Reich, T.; Arnold, T.; Geipel, G.; Bernhard, G. Spectroscopic Characterization of Alkaline Earth Uranyl Carbonates. *J. Solid State Chem.* **2005**, *178* (2), 567–577. https://doi.org/10.1016/j.jssc.2004.07.050.

(16) Amayri, S.; Arnold, T.; Foerstendorf, H.; Geipel, G.; Bernhard, G. Spectroscopic Characterization of Synthetic Becquerelite, $Ca[(UO_2)_6O_4(OH)_6]\cdot 8H_2O$, and Swartzite, $CaMg[UO_2(CO_3)_3]\cdot 12H_2O$. *Can. Mineral.* **2004**, *42*, 953–962. https://doi.org/10.2113/gscanmin.42.4.953.

(17) Arnold, T.; Baumann, N. Boltwoodite $[K(UO_2)(SiO_3OH)(H_2O)_{1.5}]$ and Compreignacite $K_2[(UO_2)_3O_2(OH)_3]_2\cdot 7H_2O$ Characterized by Laser Fluorescence Spectroscopy. *Spectrochim. Acta A* **2009**, *71* (5), 1964–1968. https://doi.org/10.1016/j.saa.2008.07.029.

(18) DeNeufville, J. P. Selective Detection of Uranium by Laser-Induced Fluorescence: A Potential Remote-Sensing Technique. 1: Optical Characteristics of Uranyl Geologic Targets. *Appl. Opt.* **1981**, *20* (8), 1279--1296. https://doi.org/10.1364/AO.20.001279.

(19) Prat, O.; Vercouter, T.; Ansoborlo, E.; Fichet, P.; Perret, P.; Kurttio, P.; Salonen, L. Uranium Speciation in Drinking Water from Drilled Wells in Southern Finland and Its Potential Links to Health Effects. *Environ. Sci. Technol.* **2009**, *43* (10), 3941–3946.

https://doi.org/10.1021/es803658e.

(20) Bernhard, G.; Geipel, G.; Reich, T.; Brendler, V.; Amayri, S.; Nitsche, H. Uranyl(VI) Carbonate Complex Formation: Validation of the $Ca_2UO_2(CO_3)_3$(Aq.) Species. *Radiochim. Acta* **2001**, *89* (8), 511–518. https://doi.org/10.1524/ract.2001.89.8.511.

(21) Shang, C.; Reiller, P. E. Determination of Formation Constants and Specific Ion Interaction Coefficients for Ca_n:$NUO_2(CO_3)_n^{(4-2n)-}$ Complexes in NaCl Solution by Time-Resolved Laser-Induced Luminescence Spectroscopy. *Dalton Trans.* **2020**, *49* (2), 466–481. https://doi.org/10.1039/c9dt03543e.

(22) Scanlan, J. P. Equilibria in Uranyl Carbonate Systems---II: The Overall Stability Constant of $UO_2(CO_3)_2^{2-}$ and the Third Formation Constant of and the Third Formation Constant of $UO_2(CO_3)_3$<sup>4. *J. Inorg. Nucl. Chem.* **1977**, *39* (4), 635–639. https://doi.org/10.1016/0022-1902(77)80578-2.

(23) Meinrath, G.; Klenze, R.; Kim, J. I. Direct Spectroscopic Speciation of Uranium(VI) in Carbonate Solutions. *Radiochim. Acta* **1996**, *74*, 81–86. https://doi.org/10.1524/ract.1996.74.special-issue.81.

(24) Jung, E. C.; Cho, H.-R.; Baik, M. H.; Kim, H.; Cha, W. Time-Resolved Laser Fluorescence Spectroscopy of $UO_2(CO_3)_3^{4-}$. *Dalton Trans.* **2015**, *44* (43), 18831–18838. https://doi.org/10.1039/C5DT02873F.

(25) Bernhard, G.; Geipel, G.; Brendler, V.; Nitsche, H. Speciation of Uranium in Seepage Waters of a Mine Tailing Pile Studied by Time-Resolved Laser-Induced Fluorescence Spectroscopy (TRLFS). *Radiochim. Acta* **1996**, *74*, 87–91.

https://doi.org/10.1524/ract.1996.74.special-issue.87.

(26) Jo, Y.; Kirishima, A.; Kimuro, S.; Kim, H. K.; Yun, J. I. Formation of $CaUO_2(CO_3)_3^{2-}$ and $Ca_2UO_2(CO_3)_3(Aq)$ Complexes at Variable Temperatures (10-70 °C). *Dalton Trans.* **2019**, *48* (20), 6942–6950. https://doi.org/10.1039/c9dt01174a.

(27) Jo, Y.; Kim, H.-K.; Yun, J.-I. Complexation of $UO_2(CO_3)_2^{4-}$ with Mg^{2+} at Varying Temperatures and Its Effect on U(VI) Speciation in Groundwater and Seawater. *Dalton Trans.* **2019**, *48* (39), 14769–14776. https://doi.org/10.1039/C9DT03313K.

(28) Endrizzi, F.; Rao, L. F. Chemical Speciation of Uranium(VI) in Marine Environments: Complexation of Calcium and Magnesium Ions with $UO_2(CO_3)_3^{4-}$ and the Effect on the Extraction of Uranium from Seawater. *Chem. Eur. J.* **2014**, *20* (44), 14499–14506. https://doi.org/10.1002/chem.201403262.

(29) Dong, W.; Brooks, S. C. Determination of the Formation Constants of Ternary Complexes of Uranyl and Carbonate with Alkaline Earth Metals (Mg^{2+}, Ca^{2+}, Sr^{2+}, and Ba^{2+}) Using Anion Exchange Method. *Environ. Sci. Technol.* **2006**, *40*, 4689–4695. https://doi.org/10.1021/es0606327.

(30) Kalmykov, S. N.; Choppin, G. R. Mixed $Ca^{2+}/UO_2^{2+}CO_3^{2-}$ Complex Formation at Different Ionic Strengths. *Radiochim. Acta* **2000**, *88* (9–11), 603–606. https://doi.org/10.1524/ract.2000.88.9-11.603.

(31) Geipel, G.; Amayri, S.; Bernhard, G. Mixed Complexes of Alkaline Earth Uranyl Carbonates: A Laser-Induced Time-Resolved Fluorescence Spectroscopic Study. *Spectrochim. Acta A* **2008**, *71* (1), 53–58. https://doi.org/10.1016/j.saa.2007.11.007.

(32) Baik, M. H.; Jung, E. C.; Jeong, J. Determination of Uranium Concentration and Speciation in Natural Granitic Groundwater Using TRLFS. *J. Radioanal. Nucl. Chem.* **2015**, *305* (2), 589–598. https://doi.org/10.1007/s10967-015-3971-2.

(33) Maloubier, M.; Solari, P. L.; Moisy, P.; Monfort, M.; Den Auwer, C.; Moulin, C. XAS and TRLIF Spectroscopy of Uranium and Neptunium in Seawater. *Dalton Trans.* **2015**, *44* (12), 5417–5427. https://doi.org/10.1039/c4dt03547j.

(34) Wang, Z. M.; Zachara, J. M.; Yantasee, W.; Gassman, P. L.; Liu, C. X.; Joly, A. G. Cryogenic Laser Induced Fluorescence Characterization of U(VI) in Hanford Vadose Zone Pore Waters. *Environ. Sci. Technol.* **2004**, *38* (21), 5591–5597. https://doi.org/10.1021/es049512u.

(35) Lee, J. Y.; Vespa, M.; Gaona, X.; Dardenne, K.; Rothe, J.; Rabung, T.; Altmaier, M.; Yun, J. I. Formation, Stability and Structural Characterization of Ternary $MgUO_2(CO_3)_3^{2-}$ and $Mg_2UO_2(CO_3)_3(Aq)$ Complexes. *Radiochim. Acta* **2017**, *105* (3), 171–185. https://doi.org/10.1515/ract-2016-2643.

(36) Beccia, M. R.; Matara-Aho, M.; Reeves, B.; Roques, J.; Solari, P. L.; Monfort, M.; Moulin, C.; Den Auwer, C. New Insight into the Ternary Complexes of Uranyl Carbonate in Seawater. *J. Environ. Radioact.* **2017**, *178*, 343–348. https://doi.org/10.1016/j.jenvrad.2017.08.008.

(37) Kalashnyk, N.; Perry, D. L.; Ivanov, V. G.; Faulques, E. Combined Experimental and First-Principles Studies of a Hydrated Uranyl Carbonate: Insight into Phonon Spectra for a Core Environmental Class of Uranium Materials. *J. Phys. Chem. Solids* **2020**, *138*, 10. https://doi.org/10.1016/j.jpcs.2019.109260.

(38) Allen, P. G.; Bucher, J. J.; Clark, D. L.; Edelstein, N. M.; Ekberg, S. A.; Gohdes, J. W.; Hudson, E. A.; Kaltsoyannis, N.; Lukens, W. W.; Neu, M. P.; Palmer, P. D.; Reich, T.; Shuh, D. K.; Tait, C. D.; Zwick, B. D. Multinuclear NMR, Raman, EXAFS, and X-Ray Diffraction Studies of Uranyl Carbonate Complexes in Near-Neutral Aqueous Solution. X-Ray Structure of $[C(NH_2)_3]_6[(UO_2)_3(CO_3)_6]\cdot 6.5H<sub$. *Inorg. Chem.* **1995**, *34*, 4797–4807. https://doi.org/10.1021/ic00123a013.

(39) Kelly, S. D.; Kemner, K. M.; Brooks, S. C. X-Ray Absorption Spectroscopy Identifies Calcium-Uranyl-Carbonate Complexes at Environmental Concentrations. *Geochim. Cosmochim. Acta* **2007**, *71* (4), 821–834. https://doi.org/10.1016/j.gca.2006.10.013.

(40) Ikeda, A.; Hennig, C.; Tsushima, S.; Takao, K.; Ikeda, Y.; Scheinost, A. C.; Bernhard, G. Comparative Study of Uranyl (VI) and-(V) Carbonato Complexes in an Aqueous Solution. *Inorg. Chem.* **2007**, *46* (10), 4212–4219. https://doi.org/10.1021/ic070051y.

(41) De Jong, W. A.; Aprà, E.; Windus, T. L.; Nichols, J. A.; Harrison, R. J.; Gutowski, K. E.; Dixon, D. A. Complexation of the Carbonate, Nitrate, and Acetate Anions with the Uranyl Dication: Density Functional Studies with Relativistic Effective Core Potentials. *J. Phys. Chem. A* **2005**, *109* (50), 11568–11577. https://doi.org/10.1021/jp0541462.

(42) Kalashnyk, N.; Perry, D. L.; Massuyeau, F.; Faulques, E. Exploring Optical and Vibrational Properties of the Uranium Carbonate Andersonite with Spectroscopy and First-Principles Calculations. *J. Phys. Chem. C* **2018**, *122* (13), 7410–7420. https://doi.org/10.1021/acs.jpcc.8b00871.

(43) Madic, C.; Hobart, D. E.; Begun, G. M. Raman Spectrometric Studies of Actinide (V) and-(VI) Complexes in Aqueous Sodium Carbonate Solution and of Solid Sodium Actinide (V)

Carbonate Compounds. *Inorg. Chem.* **1983**, *22* (10), 1494–1503. https://doi.org/10.1021/ic00152a015.

(44) Maya, L.; Begun, G. M. A Raman Spectroscopy Study of Hydroxo and Carbonato Species of the Uranyl (VI) Ion. *J. Inorg. Nucl. Chem.* **1981**, *43* (11), 2827–2832. https://doi.org/10.1016/0022-1902(81)80625-2.

(45) Doudou, S.; Arumugam, K.; Vaughan, D. J.; Livens, F. R.; Burton, N. A. Investigation of Ligand Exchange Reactions in Aqueous Uranyl Carbonate Complexes Using Computational Approaches. *Phys. Chem. Chem. Phys.* **2011**, *13* (23), 11402–11411. https://doi.org/10.1039/c1cp20617f.

(46) Kubicki, J. D.; Halada, G. P.; Jha, P.; Phillips, B. L. Quantum Mechanical Calculation of Aqueuous Uranium Complexes: Carbonate, Phosphate, Organic and Biomolecular Species. *Chem. Cent. J.* **2009**, *3* (1), 10. https://doi.org/10.1186/1752-153X-3-10.

(47) Tirler, A. O.; Hofer, T. S. Structure and Dynamics of the Uranyl Tricarbonate Complex in Aqueous Solution: Insights from Quantum Mechanical Charge Field Molecular Dynamics. *J. Phys. Chem. B* **2014**, *118* (45), 12938–12951. https://doi.org/10.1021/jp503171g.

(48) Li, B.; Zhou, J.; Priest, C.; Jiang, D. Effect of Salt on the Uranyl Binding with Carbonate and Calcium Ions in Aqueous Solutions. *J. Phys. Chem. B* **2017**, *121* (34), 8171–8178. https://doi.org/10.1021/acs.jpcb.7b04449.

(49) Tecmer, P.; Gomes, A. S. P.; Ekstrom, U.; Visscher, L. Electronic Spectroscopy of UO_2^{2+}, NUO^+ and NUN: An Evaluation of Time-Dependent Density Functional Theory for Actinides. *Phys. Chem. Chem. Phys.* **2011**, *13* (13), 6249–6259.

https://doi.org/10.1039/c0cp02534h.

(50) Oher, H.; Réal, F.; Vercouter, T.; Vallet, V. Investigation of the Luminescence of $[UO_2X_4]^{2-}$ (X = Cl, Br) Complexes in the Organic Phase Using Time-Resolved Laser-Induced Fluorescence Spectroscopy and Quantum Chemical Simulations. *Inorg. Chem.* **2020**, *59* (9), 5896–5906. https://doi.org/10.1021/acs.inorgchem.9b03614.

(51) Watkin, D. J.; Denning, R. G.; Prout, K. Structure of Dicaesium Tetrachlorodioxouranium (VI). *Acta Crystallogr. Sect. C Crystal Struct. Commun.* **1991**, *47*, 2517–2519. https://doi.org/10.1107/s0108270191006777.

(52) Su, J.; Wang, Y.-L.; Wei, F.; Schwarz, W. H. E.; Li, J. Theoretical Study of the Luminescent States and Electronic Spectra of UO_2Cl_2 in an Argon Matrix. *J. Chem. Theory Comput.* **2011**, *7* (10), 3293–3303. https://doi.org/10.1021/ct200419x.

(53) Görller-Walrand, C.; De Houwer, S.; Fluyt, L.; Binnemans, K. Spectroscopic Properties of Uranyl Chloride Complexes in Non-Aqueous Solvents. *Phys. Chem. Chem. Phys.* **2004**, *6* (13), 3292–3298. https://doi.org/10.1039/b317002k.

(54) Su, J.; Wang, Z.; Pan, D.; Li, J. Excited States and Luminescent Properties of UO_2F_2 and Its Solvated Complexes in Aqueous Solution. *Inorg. Chem.* **2014**, *53* (14), 7340–7350. https://doi.org/10.1021/ic5006852.

(55) Su, J.; Zhang, K.; Schwarz, W. H. E.; Li, J. Uranyl-Glycine-Water Complexes in Solution: Comprehensive Computational Modeling of Coordination Geometries, Stabilization Energies, and Luminescence Properties. *Inorg. Chem.* **2011**, *50* (6), 2082–2093. https://doi.org/10.1021/ic200204p.

(56) Mozhayskiy, V. A.; Krylov, A. I. EzSpectrum, Http://Iopenshell.Usc.Edu/Downloads.

(57) Docrat, T. I.; Mosselmans, J. F. W.; Charnock, J. M.; Whiteley, M. W.; Collison, D.; Livens, F. R.; Jones, C.; Edmiston, M. J. X-Ray Absorption Spectroscopy of Tricarbonatodioxouranate(V), $[UO_2(CO_3)_3]^{5-}$, in Aqueous Solution. *Inorg. Chem.* **1999**, *38*, 1879–1882. https://doi.org/10.1021/ic9814423.

(58) Ernzerhof, M.; Scuseria, G. E. Assessment of the Perdew--Burke--Ernzerhof Exchange-Correlation Functional. *J. Chem. Phys.* **1999**, *110* (11), 5029–5036. https://doi.org/10.1063/1.478401.

(59) Frisch, M. J.; Trucks, G. W.; Schlegel, H. B.; Scuseria, G. E.; Robb, M. A.; Cheeseman, J. R.; Scalmani, G.; Barone, V.; Petersson, G. A.; Nakatsuji, H.; Li, X.; Caricato, M.; Marenich, A. V; Bloino, J.; Janesko, B. G.; Gomperts, R.; Mennucci, B.; Hratchian, H. P.; Ortiz, J. V; Izmaylov, A. F.; Sonnenberg, J. L.; Williams-Young, D.; Ding, F.; Lipparini, F.; Egidi, F.; Goings, J.; Peng, B.; Petrone, A.; Henderson, T.; Ranasinghe, D.; Zakrzewski, V. G.; Gao, J.; Rega, N.; Zheng, G.; Liang, W.; Hada, M.; Ehara, M.; Toyota, K.; Fukuda, R.; Hasegawa, J.; Ishida, M.; Nakajima, T.; Honda, Y.; Kitao, O.; Nakai, H.; Vreven, T.; Throssell, K.; Montgomery Jr., J. A.; Peralta, J. E.; Ogliaro, F.; Bearpark, M. J.; Heyd, J. J.; Brothers, E. N.; Kudin, K. N.; Staroverov, V. N.; Keith, T. A.; Kobayashi, R.; Normand, J.; Raghavachari, K.; Rendell, A. P.; Burant, J. C.; Iyengar, S. S.; Tomasi, J.; Cossi, M.; Millam, J. M.; Klene, M.; Adamo, C.; Cammi, R.; Ochterski, J. W.; Martin, R. L.; Morokuma, K.; Farkas, O.; Foresman, J. B.; Fox, D. J. Gaussian˜16 {R}evision {B}.01. 2016.

(60) Pierloot, K.; van Besien, E. Electronic Structure and Spectrum of UO_2^{2+} and $UO_2Cl_4^{2-}$. *J.*

Chem. Phys. **2005**, *123* (20), 204309. https://doi.org/10.1063/1.2121608.

(61) Weigend, F.; Häser, M.; Patzelt, H.; Ahlrichs, R. RI-MP2: Optimized Auxiliary Basis Sets and Demonstration of Efficiency. *Chem. Phys. Lett.* **1998**, *294* (1–3), 143–152. https://doi.org/10.1016/S0009-2614(98)00862-8.

(62) Weigend, F.; Ahlrichs, R. Balanced Basis Sets of Split Valence, Triple Zeta Valence and Quadruple Zeta Valence Quality for H to Rn: Design and Assessment of Accuracy. *Phys. Chem. Chem. Phys.* **2005**, *7* (18), 3297–3305. https://doi.org/10.1039/B508541A.

(63) Küchle, W.; Dolg, M.; Stoll, H.; Preuss, H. Energy-Adjusted Pseudopotentials for the Actinides. Parameter Sets and Test Calculations for Thorium and Thorium Monoxide. *J. Chem. Phys.* **1994**, *100* (10), 7535–7542. https://doi.org/10.1063/1.466847.

(64) Cao, X.; Dolg, M.; Stoll, H. Valence Basis Sets for Relativistic Energy-Consistent Small-Core Actinide Pseudopotentials. *J. Chem. Phys.* **2003**, *118* (2), 487–496. https://doi.org/10.1063/1.1521431.

(65) Eichkorn, K.; Weigend, F.; Treutler, O.; Ahlrichs, R. Auxiliary Basis Sets for Main Row Atoms and Transition Metals and Their Use to Approximate Coulomb Potentials. *Theor. Chem. Acc.* **1997**, *97* (1–4), 119–124. https://doi.org/10.1007/s002140050244.

(66) Tecmer, P.; Bast, R.; Kenneth, R.; Lucas, V. Charge-Transfer Excitations in Uranyl Tetrachloride $[UO_2Cl_4]^{2-}$: How Reliable Are Electronic Spectra from Relativistic Time-Dependent Density Functional Theory? *J. Phys. Chem. A* **2012**, *116* (27), 7397–7404. https://doi.org/10.1021/jp3011266.

(67) Tecmer, P.; Govind, N.; Kowalski, K.; De Jong, W. A.; Visscher, L. Reliable Modeling of

the Electronic Spectra of Realistic Uranium Complexes. *J. Chem. Phys.* **2013**, *139* (3), 34301. https://doi.org/10.1063/1.4812360.

(68) Yanai, T.; Tew, D. P.; Handy, N. C. A New Hybrid Exchange-Correlation Functional Using the Coulomb-Attenuating Method (CAM-B3LYP). *Chem. Phys. Lett.* **2004**, *393* (1–3), 51–57. https://doi.org/10.1016/j.cplett.2004.06.011.

(69) Van Lenthe, E.; Baerends, E.-J.; Snijders, J. G. Relativistic Regular Two-Component Hamiltonians. *J. Chem. Phys.* **1993**, *99* (6), 4597–4610. https://doi.org/10.1063/1.466059.

(70) Klamt, A.; Schüürmann, G. COSMO: A New Approach to Dielectric Screening in Solvents with Explicit Expressions for the Screening Energy and Its Gradient. *J. Chem. Soc. Perkin Trans. 2* **1993**, *5*, 799–805. https://doi.org/10.1039/P29930000799.

(71) Klamt, A. Conductor-like Screening Model for Real Solvents: A New Approach to the Quantitative Calculation of Solvation Phenomena. *J. Phys. Chem.* **1995**, *99* (7), 2224–2235. https://doi.org/10.1021/j100007a062.

(72) Klamt, A.; Jonas, V. Treatment of the Outlying Charge in Continuum Solvation Models. *J. Chem. Phys.* **1996**, *105* (22), 9972–9981. https://doi.org/10.1063/1.472829.

(73) Baerends, E. J.; Ziegler, T.; Atkins, A. J.; Autschbach, J.; Bashford, D.; Baseggio, O.; Bérces, A.; Bickelhaupt, F. M.; Bo, C.; Boerritger, P. M.; Cavallo, L.; Daul, C.; Chong, D. P.; Chulhai, D. V; Deng, L.; Dickson, R. M.; Dieterich, J. M.; Ellis, D. E.; van Faassen, M.; Ghysels, A.; Giammona, A.; van Gisbergen, S. J. A.; Goez, A.; Götz, A. W.; Gusarov, S.; Harris, F. E.; van den Hoek, P.; Hu, Z.; Jacob, C. R.; Jacobsen, H.; Jensen, L.; Joubert, L.; Kaminski, J. W.; van Kessel, G.; König, C.; Kootstra, F.; Kovalenko, A.; Krykunov, M.;

van Lenthe, E.; McCormack, D. A.; Michalak, A.; Mitoraj, M.; Morton, S. M.; Neugebauer, J.; Nicu, V. P.; Noodleman, L.; Osinga, V. P.; Patchkovskii, S.; Pavanello, M.; Peeples, C. A.; Philipsen, P. H. T.; Post, D.; Pye, C. C.; Ramanantoanina, H.; Ramos, P.; Ravenek, W.; Rodríguez, J. I.; Ros, P.; Rüger, R.; Schipper, P. R. T.; Schlüns, D.; van Schoot, H.; Schreckenbach, G.; Seldenthuis, J. S.; Seth, M.; Snijders, J. G.; Solà, M.; M., S.; Swart, M.; Swerhone, D.; te Velde, G.; Tognetti, V.; Vernooijs, P.; Versluis, L.; Visscher, L.; Visser, O.; Wang, F.; Wesolowski, T. A.; van Wezenbeek, E. M.; Wiesenekker, G.; Wolff, S. K.; Woo, T. K.; Yakovlev, A. L. ADF2018, SCM, Theoretical Chemistry, Vrije Universiteit, Amsterdam, The Netherlands, Https://Www.Scm.Com.

(74) Van Lenthe, E.; Baerends, E. J. Optimized Slater-Type Basis Sets for the Elements 1-118. *J. Comput. Chem.* **2003**, *24* (9), 1142–1156. https://doi.org/10.1002/jcc.10255.

(75) Réal, F.; Vallet, V.; Marian, C.; Wahlgren, U. Theoretical Investigation of the Energies and Geometries of Photoexcited Uranyl(VI) Ion: A Comparison between Wave-Function Theory and Density Functional Theory. *J. Chem. Phys.* **2007**, *127* (21), 214302. https://doi.org/10.1063/1.2814157.

(76) Parkhurst, D. L.; Appelo, C. A. J. User's Guide to PHREEQC (Version 2) — A Computer Program for Speciation, Batch-Reaction, One-Dimensional Transport, and Inverse Geochemical Calculations. U.S. Geological Survey, Water-Resources Investigations: Lakewood, Colorado, USA 1999.

(77) Guillaumont, R.; Fanghänel, T.; Fuger, J.; Grenthe, I.; Neck, V.; Palmer, D. A.; Rand, M. H. Update on the Chemical Thermodynamics of Uranium, Neptunium, Plutonium, Americium and Technetium, Chemical Thermodynamics. *Nucl. Energy Agency, Elsevier*

Sci. Publ. 918.

(78) Lee, J. Y.; Vespa, M.; Gaona, X.; Dardenne, K.; Rothe, J.; Rabung, T.; Altmaier, M.; Yun, J. Il. Formation, Stability and Structural Characterization of Ternary $MgUO_2(CO_3)_3^{2-}$ and $Mg_2UO_2(CO_3)_3(Aq)$ Complexes. *Radiochim. Acta* **2017**, *105* (3), 171–185. https://doi.org/10.1515/ract-2016-2643.

(79) Shannon, R. D. Effective Ionic Radii and Systematic Studies of Interatomic Distances in Halides and Chaleogenides. *Acta Crystallogr. A* **1976**, *32*, 751–767. https://doi.org/10.1107/S0567739476001551.

(80) Anderson, A.; Chieh, C.; Irish, D. E.; Tong, J. P. K. An X-Ray Crystallographic, Raman, and Infrared Spectral Study of Crystalline Potassium Uranyl Carbonate, $K_4UO_2(CO_3)_3$. *Can. J. Chem.* **1980**, *58* (16), 1651–1658. https://doi.org/10.1139/v80-264.

(81) Parr, R. G.; Pearson, R. G. Absolute Hardness: Companion Parameter to Absolute Electronegativity. *J. Am. Chem. Soc.* **1983**, *105* (26), 7512–7516. https://doi.org/10.1021/ja00364a005.

(82) Clugston, M. J.; Flemming, R. *Advanced Chemistry*; Oxford University Press: Oxford New York, 2000.

(83) Nizhegorodov, N. I. Effect of Molecule Symmetry on Fluorescence Parameters and on the Intercombination Conversion Constant. *J. Appl. Spectrosc.* **1992**, *57* (5), 873–878. https://doi.org/10.1007/BF00663933.

(84) Lakowicz, J. R. *Principles of Fluorescence Spectroscopy*, 3rd ed.; Springer: New York, 2006.

(85) Drobot, B.; Steudtner, R.; Raff, J.; Geipel, G.; Brendler, V.; Tsushima, S. Combining Luminescence Spectroscopy, Parallel Factor Analysis and Quantum Chemistry to Reveal Metal Speciation--a Case Study of Uranyl (VI) Hydrolysis. *Chem. Sci.* **2015**, *6* (2), 964–972. https://doi.org/10.1039/C4SC02022G.

(86) Moulin, C.; Decambox, P.; Mauchien, P.; Pouyat, D.; Couston, L. Direct Uranium (VI) and Nitrate Determinations in Nuclear Reprocessing by Time-Resolved Laser-Induced Fluorescence. *Anal. Chem.* **1996**, *68* (18), 3204–3209. https://doi.org/10.1021/ac9602579.